Recent advances in nanomaterial-modified polyamide thin-film composite membranes for forward osmosis processes

Nawshad Akther[a], Sherub Phuntsho[a], Yuan Chen[b], Noreddine Ghaffour[c], and Ho Kyong Shon*[a]

Journal Name: Journal of Membrane Science

Date: 15th March 2019

[a]Centre for Technology in Water and Wastewater (CTWW), School of Civil and Environmental Engineering, University of Technology Sydney (UTS), NSW 2007, Australia

[b]The University of Sydney, School of Chemical and Biomolecular Engineering, Sydney, NSW, 2006, Australia

[c]King Abdullah University of Science and Technology (KAUST), Water Desalination and Reuse Center (WDRC), Biological & Environmental Science & Engineering Division (BESE), Thuwal, 23955-6900, Saudi Arabia

*Corresponding author: Prof. Ho Kyong Shon Email: hokyong.shon-1@uts.edu.au

Abstract

Polyamide thin-film composite (PA TFC) membranes have attained much attention for forward osmosis (FO) applications in separation processes, water and wastewater treatment due to their superior intrinsic properties, such as high salt rejection and water permeability compared to the first generation of cellulose-based FO membranes. Nonetheless, several problems like fouling and trade-off between membrane selectivity and water permeability are hindering the progress of conventional PA TFC FO membranes for real applications. To overcome these issues, nanomaterials or chemical additives have been integrated into the TFC membranes. Nanomaterial-modified membranes have demonstrated significant improvement in their anti-fouling properties and FO performance. In addition, PA TFC membranes can be designed for specific applications like heavy metal removal and osmotic membrane bioreactor by using nanomaterials to modify their physicochemical properties (porosity, surface charge, hydrophilicity, membrane structure and mechanical strength). This review provides a comprehensive summary of the progress of nanocomposite PA TFC membrane since its first development for FO in the year 2012. The nanomaterial-incorporated TFC membranes are classified into four categories based on the location of nanomaterial in/on the membranes: embedded inside the PA active layer, incorporated within the substrate, coated on the PA layer surface, or deposited as an interlayer between the substrate and the PA active layer. The key challenges still being confronted and the future research directions for nanocomposite PA TFC FO are also discussed.

Keywords: Forward osmosis membrane, thin-film composite (TFC), thin-film nanocomposite (TFN), nanoparticles, interfacial polymerization

Contents

1. Introduction 5
2. Nanomaterial-modified PA active layers 11
2.1 Zeolites and silica 17
2.2 Carbon nanotubes and graphene oxide 18
2.3 Other carbon-based nanomaterials 22
2.4 Titanate and halloysite nanotubes 24
2.5 Porous coordination polymers 26
2.6 Issues and challenges of nanomaterial-modified PA layers 28
3. Nanomaterial-coated PA layer surfaces 29
3.1 Carbon nanotubes and graphene oxide 32
3.2 Silver nanoparticles and nanocomposites 34
3.3 Membrane surface mineralization 38
3.4 Issues and challenges of nanomaterial-coated PA layer surfaces 40
4. Nanomaterial-modified substrates 41
4.1 Zeolites, silica and zinc oxide 48
4.2 Carbon nanotubes and graphene oxide 50
4.3 Titanium oxide 54
4.4 Other nanomaterials 55
4.5 Issues and challenges of nanomaterial-modified substrates 59
5. Nanomaterial interlayer 60
5.1 Carbon nanotubes and graphene oxide 61
5.2 Porous coordination polymers 63
5.3 Issues and challenges of nanomaterial interlayer 63
6. Implications and future perspectives 63
7. Conclusions 68
Acknowledgments 70
References 71

Abbreviations: 3HBTC, silver (I) and 1,3,5-benzene tricarboxylic acid; A, water permeability coefficient; AAPTS, 1-(2-amino-ethyl)-3-aminopropyl] trimethoxysilane; Ag, silver; AgNP, silver nanoparticle; AgCl, silver chloride; $AgNO_3$, silver nitrate; AL-DS, active layer facing draw solution; AL-FS, active layer facing feed solution; Al_2O_3, aluminium oxide; ASP, alternate soaking process; B, solute permeability coefficient; BaCl, barium chloride; $BaSO_4$, barium sulfate; BP, bucky paper; BSA, bovine serum albumin; C60@PAF900, fullerene impregnated porous aromatic framework; $CaCO_3$, calcium carbonate; CFV, cross-flow velocity; CN, graphitic carbon nitride; CNT, carbon nanotube; COF, covalent-organic framework; CP, concentration polarization; CSA, camphorsulfonic acid; CTA, cellulose triacetate; DA, dopamine; DS, draw solution; ECP, external concentration polarisation; EDC, n-(3-Dimethylaminopropyl)-n'-ethylcarbodiimide hydrochloride; Fe_3O_4, iron (III) oxide, FO, forward osmosis; FRR, flux recovery ratio; FS, feed solution; *f*-SWNTs, functionalized single-walled carbon nanotubes; gMH, $gm^{-2}h^{-1}$; GO, graphene oxide; HA, humic acid; GQDs, graphene quantum dots; HTI, Hydration Technologies Inc.; HNT, halloysite nanotube; ICP, internal concentration polarisation; INT, imogolite nanotube; IP, interfacial polymerization; Js, solute flux; Jw, water flux; LbL, layer-by-layer; LDH, layered double hydroxide; LMH, $Lm^{-2}h^{-1}$; MD, membrane distillation; MF, microfiltration; MOF, metal-organic framework; MPD, m-phenylenediamine; mPDA, 1,3-phenylenediamine; MWCNT, multi-walled carbon nanotube; $NaBH_4$, sodium borohydride; NaCl, sodium chloride; Na_2SO_4, sodium sulfate; NF, nanofiltration; NHS, *n*-hydroxysuccinimide; NP, nanoparticles; PA, polyamide; PAN, polyacrylonitrile; pDA, polydopamine; PEG, polyethylene glycol; PEI, polyethylenimine; PES, polyether sulfone; PET, polyester; PI, phase inversion; PLL, poly L-Lysine; PMR, photocatalytic membrane reactor; PSf, polysulfone; PV, pervaporation; PVDF, polyvinylidene fluoride; PVP, polyvinylpyrrolidone; rGO, reduced graphene oxide; RO, reverse osmosis; S, structural parameter; SA, sodium alginate; SDS, sodium dodecyl sulfate; SiO_2, silica; SRSF, specific reverse solute flux; TEA, triethylamine; TFC, thin-film composite; TFN, thin-film nanocomposite; TiO_2, titanium oxide; TMC, trimesoyl chloride; TNT, titanate nanotubes; UF, ultrafiltration; UiO-66, WW, wastewater; zirconium (IV) carboxylate metal-organic framework; Zn_2GeO_4, zinc germinate; ZnO, zinc oxide; ZSCSNP, ZnO-SiO_2 core-shell nanoparticles

1. Introduction

Membrane technologies like reverse osmosis (RO) and forward osmosis (FO) have attracted enormous research interest as more energy-efficient and sustainable methods for desalination, wastewater treatment and separation processes over the past decades [1-3]. They are simple to install and operate, highly scalable, consume relatively low energy, and their performance mechanism is well-understood [4-6]. RO is the most commonly used membrane technology as it produces the best water quality compared to other commercial membrane-based technologies like ultrafiltration (UF) and nanofiltration (NF) [7]. However, RO is a very energy-intensive process, where membrane replacement can be costly and membrane scaling and fouling can be a significant challenge [8, 9].

On the other hand, FO has turned out to be an active research area as a prospective low-energy membrane-separation technology, mainly for application in wastewater treatment, RO pre-treatment and brine dilution [10, 11]. Unlike RO, which operates at a very high hydraulic pressure, FO processes are driven naturally by the osmotic pressure difference existing between the draw and feed solution with the existence of little or zero transmembrane pressure [12]. In a FO process, water moves from a low concentrated feed to a highly concentrated draw solution through a semi-permeable membrane, while rejecting solutes on both sides of the membrane. Pure water is then separated from the diluted draw solution using a suitable separation technique [13, 14]. However, the draw solute regeneration step in the FO process is significantly energy-intensive, which makes direct desalination with RO more energy-efficient than FO [15]. Nonetheless, FO may be more energetically favorable than RO for high salinity and high fouling potential applications that do not require draw solution regeneration, such as food concentration and brine dilution [16, 17].

Besides, FO processes can remove an extensive range of pollutants present in the feed solution [18], and function at much greater feed recovery rates than the RO processes [19]. FO membranes have higher fouling reversibility than the pressure-driven RO process, and most FO foulants can generally be removed by physical cleaning requiring only limited chemical cleaning frequency [20-22]. However, membrane characteristics play a significant role in the process performance and the economics of the FO technology in addition to the other factors, such as draw solution type and regeneration method [11].

Development of FO membranes started around the year 2000. Prior to that, FO studies were conducted mostly using RO membranes, which were unsuitable for FO applications due to their thick support layers. For a FO process to work efficiently, it is desirable that the membranes exhibit high water flux, low reverse solute flux, excellent mechanical stability, chemical resistance and antifouling property [10]. McCutcheon and Elimelech concluded based on the results from their asymmetric membrane flux modeling that FO membranes should have smaller solute resistance to diffusion (K) values to diminish the internal concentration polarisation (ICP) effect and achieve high water flux during the FO operation [23-25]. The K values could be improved by increasing the membrane porosity and reducing membrane thickness. The first generation FO membrane commercialized by Hydration Technologies, Inc. (HTI) comprised of cellulose triacetate (CTA) supported on a thin woven polyester mesh [26]. Although the commercial CTA FO membranes were able to reduce the ICP effects, the water permeability and selectivity of the CTA membranes were not impressive [27]. HTI later developed a thin-film composite (TFC) FO membrane that included a thin polyamide (PA) selective layer on top of a porous substrate layer supported by a polyester (PET) mesh. The HTI TFC membrane demonstrated a much higher solute rejection and a water flux nearly double of that achieved using CTA FO membrane [28]. Unlike the CTA membranes, which can operate under a limited pH range of 4 to 8 [29], the TFC membranes

158 can tolerate a wide pH range of 2 to12 and have better chemical stability [27]. The high
159 biodegradability of CTA membrane reduces its membrane lifespan; thereby, limiting its
160 application [10]. As a result, most recent studies on FO membranes are aimed towards TFC
161 membrane fabrication and their modification.

162 Polymeric TFC membranes have been previously used for NF and RO applications, and
163 they usually involve the development of a thin dense active layer on top of a porous substrate
164 [30, 31]. The thin selective or active layer is usually formed by interfacial polymerization (IP)
165 reaction of monomers, and its thin-film formation is significantly governed by the structure
166 and properties of the membrane substrate [32-34]. The substrate structure and morphology
167 significantly influence the degree of ICP within the porous layer [35]; whereas, the active layer
168 controls the extent of solute and water fluxes across the membrane [36]. Additionally,
169 membrane fouling lowers water flux by increasing membrane resistance, which further reduces
170 the mass transfer coefficient and enhances external concentration polarization (ECP) on the
171 membrane surface [37-40]. Although PA-based TFC FO membranes have better performance
172 compared to the cellulose-based membranes, the overall FO performance in terms of ICP,
173 fouling resistance and chlorine tolerance is still an issue [11].

174 Inspired by nanocomposite membranes developed in the 1990s for gas separation [41],
175 several studies have incorporated nanomaterials in RO and FO membranes to improve the
176 overall membrane performance as reviewed by Li, Yan and Wang [42]. Xiao et al. developed
177 a general multiscale modeling and simulation framework to predict the properties of polymer
178 nanocomposites like mechanical strength and permeability for gas separation [43]. The
179 framework could be used to investigate the molecular level interactions between thermoset
180 polymer and various types of nanoparticles that affect the performance of polymer
181 nanocomposites. Nanomaterial incorporation has shown to enhance not only the water
182 permeability, antimicrobial properties, fouling and chlorine resistance of the membranes, but

183 also their thermal stability and mechanical strength. Silver nanoparticles have been extensively
184 used as an antimicrobial agent in nanocomposite membranes to improve their antimicrobial
185 properties [44]. Whereas, the addition of porous nanoparticles like zeolites were found to
186 increase the water permeability of the nanocomposite membranes by creating channels for
187 water transport [45]. The changes in properties of nanocomposite membranes are strongly
188 influenced by the chemical properties, type, size and concentration of the nanomaterial used.
189 As such, the nanocomposite membrane properties can be tailored depending on the type of
190 nanomaterial chosen. The first nanocomposite FO membrane with improved water
191 permeability was developed by Tang's group in 2012 [45], which was inspired by the study on
192 zeolite-incorporated TFC RO membrane [46]. The increasing interest in the development of
193 nanomaterial-based PA TFC FO membranes is evident from the increasing number of studies
194 published as presented in Figure 1.

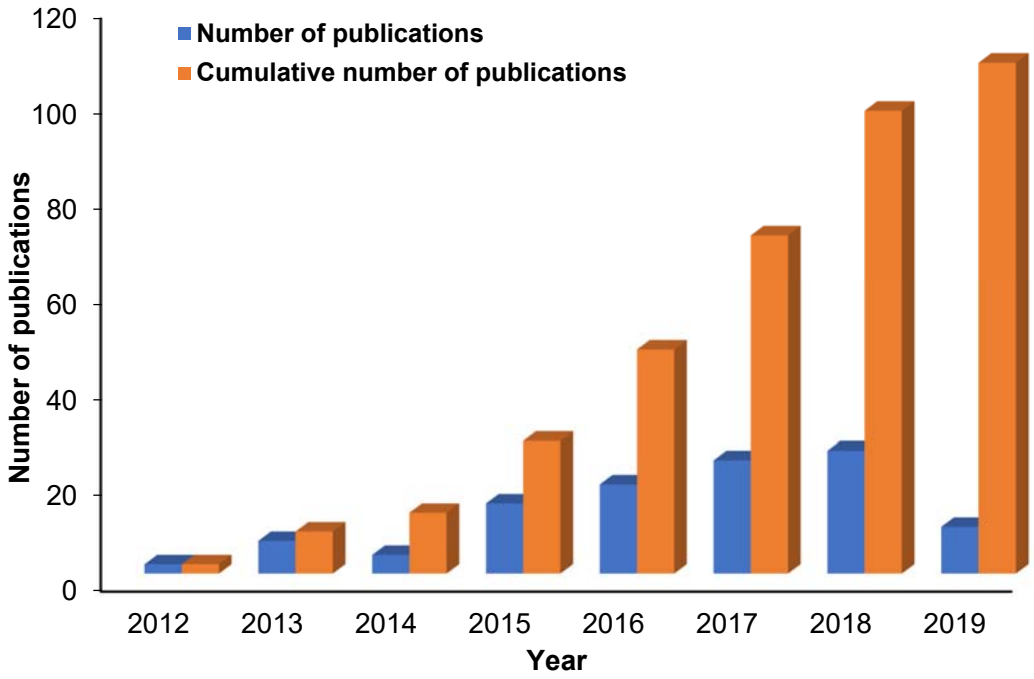

195

196 Figure 1: Number of publications related to nanomaterial-modified PA TFC FO membranes (Retrieved from Web
197 of Science on 14th March 2019).

Nanomaterials can be added either into the active layer or into the substrate of the membrane to enhance active layer's transport properties, substrate's structural characteristics, and membrane's overall mechanical stability and chemical resistance [42]. Some studies have also coated or covalently bonded nanomaterials on the membrane surface to improve membrane hydrophilicity, surface charge density and antifouling property [47, 48]. Whereas, others have deposited nanomaterial interlayer on porous substrates for formation of defect-free PA active layer [49, 50]. Based on the approach of nanomaterial integration, TFC membranes can be classified as follows: (a) thin-film nanocomposite (TFN) membrane, (b) TFC membrane with a nanomaterial-coated PA layer surface, (c) TFC membrane with a nanocomposite substrate, and (d) TFC membrane with a nanomaterial interlayer (Figure 2). Some of the inorganic nanomaterials that have been most widely used for FO membrane modification include zeolite [45, 51], graphene oxide (GO) [52-54], carbon nanotubes (CNTs) [55-58], silica [59, 60] and titanium oxide [61-63].

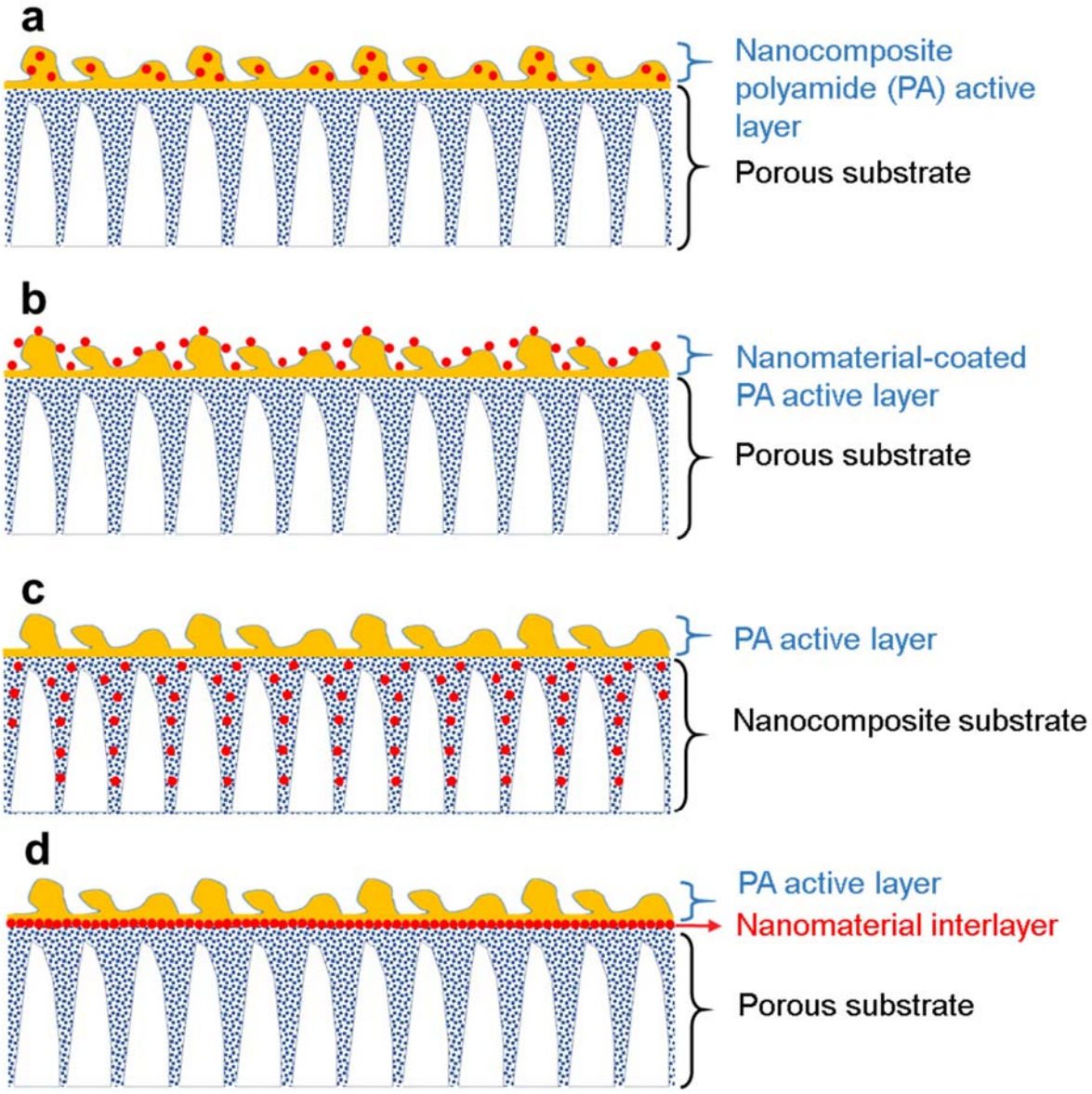

Figure 2: Schematic illustrations demonstrating typical structures of nanomaterial-incorporated PA TFC membranes: a) TFN membrane, b) TFC membrane with nanomaterial-coated PA layer surface, c) TFC membrane with nanocomposite substrate and d) TFC membrane with nanomaterial interlayer.

The review articles on FO membranes that have been published to date have considered draw solutes [64-66], membrane fouling [39, 67, 68], various FO applications [69-72], FO membrane materials, fabrication methods and their chemical modifications [73-75]. However, a specialized review providing ample information on the advancement of nanomaterial-

221 incorporated PA TFC membranes for FO applications is currently lacking. The development
222 of high-performing FO membranes, especially those incorporated with nanoparticles, has
223 gained significant research interests recently as they have the potential to enhance FO
224 performance. Hence, for the first time, we set out to provide a comprehensive review on the
225 progress and developments of incorporating various kinds of nanomaterials into the active
226 layer, substrate and surface of PA TFC FO membranes. The major challenges, future research
227 directions and prospects in the development of nanomaterial-incorporated PA TFC membrane
228 are also critically discussed. The aquaporin-based biomimetic FO membranes have not been
229 included in this review due to the difference in their fabrication technique and behavior from
230 that of the nanocomposite PA TFC membranes. Habel et al. provided an extensive review of
231 the different fabrication and characterization approaches for aquaporin-based biomimetic
232 membranes [76]. This review is expected to inspire more studies to address the existing
233 challenges in membrane development and realize the practical applications of membranes for
234 enhancing FO performance.

235 2. Nanomaterial-modified PA active layers

236 Since 2012, several studies have dispersed inorganic nanomaterials into the thin PA
237 active layer of the TFC FO membranes to improve their separation performance. The PA layer
238 is made via IP reaction between trimesoyl chloride (TMC) organic solution and m-
239 phenylenediamine (MPD) aqueous solution. Depending on the hydrophilic/hydrophobic nature
240 of the nanofillers, they can be distributed in either aqueous MPD or organic TMC phase. Figure
241 3 illustrates the typical steps involved in the TFN membrane fabrication process. Nanomaterials
242 like zeolites, silica, GO, CNTs that have been previously used for RO nanocomposite
243 membranes have also been studied for preparation of TFN FO membranes [42, 77]. Table 1
244 and

245 Table 2 list the research articles based on the development of PA TFN membranes.

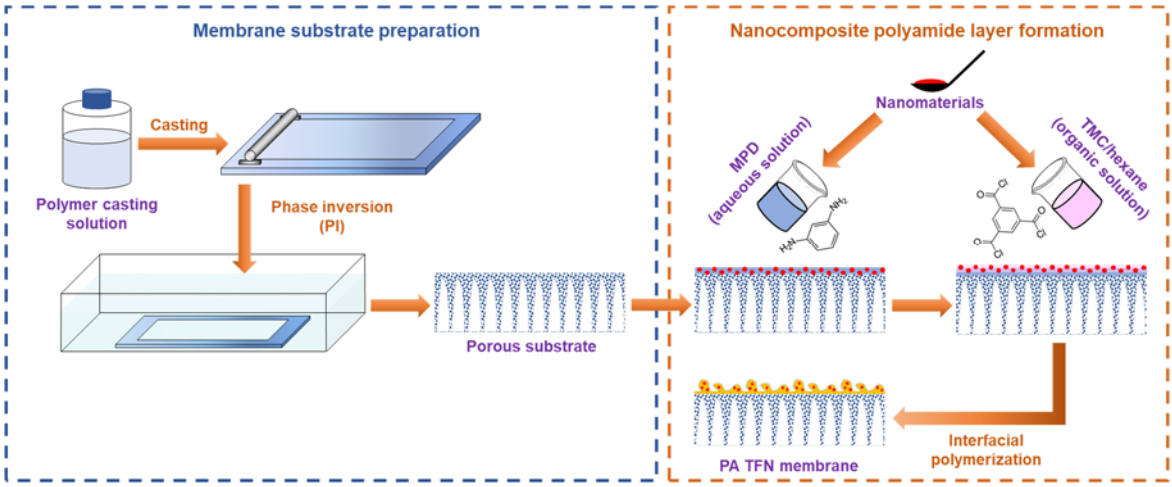

246

247 Figure 3: Typical steps involved in the fabrication of a TFN membrane through the IP process.

248 Nanomaterials are uniformly-dispersed either in the MPD aqueous or TMC organic solution

249 for the formation of nanocomposite PA layer.

250 Table 1: Summary of the fabrication conditions and FO performance of porous nanomaterial-incorporated PA TFN membranes

TFN membrane		Optimal particle loading	Intrinsic properties	Substrate fabrication method & conditions	FO performance (AL-FS)				Year [Ref]
Fillers embedded in PA layer (Particle size)	**Substrate (PA layer monomers)**				**DS (FS)**	**CFV**	**Jw (LMH)**	**Js (gMH)**	
Zeolite (NaY) (40-150 nm)	PSf (MPD, TMC)	0.1 wt/v% in TMC/n-hexane	A = 2.59 LMH/bar B = 1.57 LMH S = 782 μm	PI Casting/overall thickness = 150/70 μm	1 M NaCl (10 mM NaCl)	20 cm/s	14.6	3.5	2012 [45]
Amine functionalized CNTs (OD: 5 nm, ID: 1.3-2 nm, L: 50 μm)	PSf (MPD, TMC)	0.05 wt% in MPD solution	A = 3.56 LMH/bar B = 0.10 LMH S = 380 μm	PI Casting/overall thickness = n/a	2 M NaCl (10 mM NaCl)	7.2 cm/s	30.0	2.4	2013 [78]
CNTs (D: 20 nm, L: 0.5-2 μm)	PSf (DA Tris buffer solution, TMC)	0.05 wt/v% in DA solution	-	PI Casting/overall thickness = n/a	2 M $MgCl_2$ (DI water)	1.59 cm/s	8.6	2.1	2015 [79]
Amine functionalized TNTs (ID: 5-25 nm)	PSf (MPD, TMC)	0.05 wt/v% in TMC/cyclohexane solution	A = 2.38 LMH/bar B = 0.37 LMH S = 368 μm	PI Casting/overall thickness = n/a	1 M NaCl (10 mM NaCl)	32.72 cm/s	20.8	4.3	2015 [80]
HNTs (ID: 10-15 nm)	PSf (MPD, TMC)	0.05 wt/v% in TMC/cyclohexane solution	A = 1.87 LMH/bar B = 0.63 LMH	PI Casting/overall thickness = n/a	2 M NaCl (10 mM NaCl)	350 mL/min	20.1	5.8	2015 [81]
TiO_2/HNT nanocomposites (ID: 5-15 nm)	PSf (MPD, TMC)	0.05 wt/v% in TMC/cyclohexane solution	A = 2.45 LMH/bar B = 0.60 LMH	PI Casting/overall thickness = 120/70-90 μm	2 M NaCl (10 mM NaCl)	350 mL/min	25.5	4.9	2015 [82]
CNTs (D: 20 nm, L: 0.5-2 μm)	PSf (DA Tris buffer solution, MPD, TMC)	0.05 wt% in DA solution	A = 6.7 LMH/bar B = 8.3 LMH S = 1637 μm	PI Casting thickness = 80 μm	2 M $MgCl_2$ (DI water)	7.8 cm/s	14.5	7.5	2016 [83]

Al_2O_3 (<50 nm)	PSf, 0.5 wt% Al_2O_3 (MPD, TMC)	0.05 wt% in TMC/n-hexane solution	A = 8.43 LMH/bar B = 1.66 LMH S = 1028 µm	PI Casting thickness = 90 µm	1 M NaCl (DI water)	18.5 cm/s	27.6	7.1	2017 [84]
MOF: UiO-66 (n/a)	PSf (MPD, TMC)	0.1 wt% in TMC/ n-hexane solution	A = 3.3 LMH/bar B = 0.3 LMH S = 1637 µm	PI Casting/overall thickness = 150/62 µm	2 M NaCl (DI water)	1.1 cm/s	27.0	6.1	2017 [85]
MOF (D: 30 nm)	PES (MPD, TMC)	0.04 wt/v% in TMC/n-hexane solution	A = 4.7 LMH/bar B = 0.6 LMH S = 238 µm	PI Casting thickness = 100 µm	2 M NaCl (DI water)	21 cm/s	46.0	102.3	2017 [86]
Zwitterion (AEPPS) (n/a)	PSf (MPD, TMC)	30 wt% in MPD solution	A = 4.81 LMH/bar B = 0.19 LMH S = 747 µm	PI Casting/overall thickness = n/a	2 M NaCl (n/a)	n/a	22.5	12.5	2018 [87]
COF: SNW-1 (D: ~30 nm)	PSf (MPD, TMC)	0.005 wt% in MPD solution	A = 1.77 LMH/bar B = 0.46 LMH	PI Casting/overall thickness = 120/58 µm	1 M NaCl (DI water)	12.6 cm/s	15.6	4.8	2019 [88]

A: water permeability coefficient; Al_2O_3: aluminium oxide; B: solute permeability coefficient; CFV: cross-flow velocity; CNT: carbon nanotube; COF: covalent-organic framework; DA: dopamine; DS: draw solution; FS: feed solution; Js: solute flux; Jw: water flux; HNT: halloysite nanotube; MOF: metal-organic framework; MPD: m-phenylenediamine; PI: phase inversion; PSf: polysulfone; S: structural parameter; SNW-1: Schiff base network-1; TMC: trimesoyl chloride; TNT: titanate nanotubes

255 Table 2: Summary of the fabrication conditions and FO performance of non-porous nanomaterial-incorporated PA TFN membranes

TFN membrane		Optimal particle loading	Intrinsic properties	Substrate fabrication methods and conditions	FO performance (AL-FS)				Year [Ref]
Fillers embedded in PA layer (Particle size)	**Substrate (PA layer monomers)**				**DS (FS)**	**CFV**	**Jw (LMH)**	**Js (gMH)**	
SiO_2 (15-20 nm)	PSf (MPD, TMC)	0.05 wt% in MPD solution	A = 3.43 LMH/bar B = 1.02 LMH S = 368 µm	PI Casting thickness = 100 µm	2 M NaCl (10 mM NaCl)	800 mL/min	15.0	1.6	2014 [89]
GO (Lateral size: 35-90 nm, T: 0.75-1.25 nm)	PAN (MPD, TMC)	0.06 wt% in MPD solution	A = 2.0 LMH/bar B = 0.8 LMH S = 85 µm	PI Casting thickness = 100 µm	1 M NaCl (DI water)	300 mL/min	23.6	4.4	2016 [90]
TiO_2 (20 nm)	PSf (MPD, TMC)	0.05 wt/v% in MPD solution	A = 3.89 LMH/bar B = 1.33 LMH S = 650 ± 70 µm	PI Casting thickness = 100 µm	2 M NaCl (10 mM NaCl)	800 mL/min	20.8	8.8	2016 [62]
TiO_2 (n/a)	PSf (MPD, TMC)	0.05 wt/v% in TMC/n-hexane solution	n/a	n/a	2 M NaCl (10 mM NaCl)	300 mL/min	26.0	4.98	2016 [91]
PVP modified GO (T: 0.55-1.2 nm)	PSf (MPD, TMC)	0.0175 wt% in MPD solution	-	PI Casting thickness = 175 µm	2 M NaCl (10 mM NaCl)	333.3 mL/min	14.6	14.6	2017 [92]
Polyrhodanine (50 nm)	PES (MPD, TMC)	0.01 wt/v% in TMC/n-hexane solution	A = 1.60 LMH/bar B = 0.22 LMH S = 128 µm	PI Casting/overall thickness = n/a	1.5 M NaCl (DI water)	20 cm/s	41.0	6.7	2018 [93]
Fe_3O_4/ZnO (n/a)	PSf, 0.2 wt% Fe_3O_4/ZnO (MPD, TMC)	0.02 wt/v% in MPD solution	A = 2.97 LMH/bar B = 0.28 LMH S = 400 µm	PI Casting/overall thickness = 100/131 µm	2 M NaCl (10 mM NaCl)	720.7 cm/s	29.3	5.6	2018 [94]
GO (Flake size: 57.3 nm)	PSf (MPD, TMC)	0.1 wt% in MPD, TEA and SDS solution	A = 2.35 LMH/bar B = 0.67 LMH S = 570 µm	PI Casting thickness = 100 µm	1 M NaCl (DI water)	25 L/min	14.5	2.6	2018 [95]
GO/Fe_3O_4 nanohybrid (n/a)	PES (MPD, TMC)	0.02 wt/v% in MPD solution	A = 2.51 LMH/bar B = 0.27 LMH	PI Casting/overall thickness = 80/65 µm	1 M NaCl (DI water)	8 cm/s	27.5	3.0	2018 [96]

Fullerenol (D: ~1 nm)	PSf (MPD, TMC)	0.04 wt/v% in MPD solution	A = 3.87 LMH/bar B = 0.59 LMH	PI Casting/overall thickness = n/a	1 M NaCl (DI water)	6.4 cm/s	26.1	4.7	2018 [97]
Graphitic carbon nitride (g-C3N4) (n/a)	PSf, 0.5 wt% HNTs (MPD, TMC)	0.05 wt/v% in MPD solution	A = 2.17 LMH/bar B = 0.38 LMH S = 370 µm	PI Casting thickness = 140 µm	2 M NaCl (DI water)	21.4 cm/s	18.9	2.74	2018 [98]
GQDs (3.4-8.8 nm)	PES (MPD, TMC)	0.1 wt% in MPD, TEA and CSA solution	A = 3.35 LMH/bar B = 0.26 LMH S = 189 µm	PI Casting/overall thickness = n/a	1 M NaCl (DI water)	8.5 cm/s	28	5.84	2018 [99]
C60@PAF900 (n/a)	PSf (MPD, TMC)	0.015 wt/v% in TMC/n-hexane solution	A = 3.19 LMH/bar B = 0.66 LMH	PI Casting thickness = 175 µm	2 M NaCl (10 mM NaCl)	n/a	12.4	10.4	2018 [100]

A: water permeability coefficient; B: solute permeability coefficient; C60@PAF900: fullerene impregnated porous aromatic framework; CFV: cross-flow velocity; CNT: carbon nanotube; CSA: camphorsulfonic acid; DS: draw solution; Fe_3O_4: iron (III) oxide, FS: feed solution; GO: graphene oxide; GQDs: graphene quantum dots; Js: solute flux; Jw: water flux; MPD: m-phenylenediamine; PAN: polyacrylonitrile; PES: polyether sulfone; PI: phase inversion; PSf: polysulfone; S: structural parameter; SDS: sodium dodecyl sulfate; SiO_2: silica; TEA: triethylamine; TiO_2: titanium oxide; TMC: trimesoyl chloride

2.1 Zeolites and silica

Zeolites are microporous aluminosilicate materials with a porous crystalline structure that act as molecular sieves. The uniform and well-defined pore system of zeolites can be customized to facilitate size or shape selective separation of molecules. Additionally, zeolites are both chemically and thermally stable; hence, zeolites have been utilized extensively for membrane development in applications like pervaporation, membrane reactors, reverse osmosis and gas separation [101].

Motivated by the zeolite-incorporated TFN RO membrane, Tang's group was the first to develop TFN membrane for FO application by loading zeolite NaY nanoparticles in the range of 0.02-0.4 wt/v% into TMC/n-hexane organic solution [45]. The membrane water flux improved with increasing zeolite loading between 0.02 to 0.1 wt/v% but decreased when zeolite loading exceeded 0.1 wt/v%. The membrane with a zeolite loading of 0.1 wt/v% (TFN0.1) was found to be optimal. TFN0.1 exhibited a water flux of around 15 LMH (32 LMH) in AL-FS (AL-DS) orientation; whereas, a water flux of about 10 LMH (22 LMH) was obtained using TFC membrane when 1 M and 10 mM NaCl were used as the draw and feed solution, respectively. The authors attributed the improvement in membrane water permeability within the range of 0.02–0.1 wt/v% zeolite loading to the porous structure of zeolite. However, increasing the zeolite loading beyond 0.1 wt/v% resulted in thicker PA layer formation causing the water permeability to decrease. Nonetheless, the authors did not comment on the homogeneity of zeolite dispersion within the PA layer, which may have an impact on FO performance.

Similar to zeolites, silica incorporated membranes have been applied in many areas like gas separation, RO, NF and FO owing to its distinctive properties like high specific surface area, good surface hydrophilicity from the presence of silicon hydroxyl groups, and uniform

nanostructures that can be controlled for size selectivity [102]. In addition, silica particles have a spherical morphology, which allows them to disperse more effectively compared to zeolites.

Niksefat et al. [89] explored the influence of silica nanoparticles on the characteristics and FO performance of TFN membranes. It was reported that increasing silica concentration (0.01, 0.05 and 0.1 wt/v%) in MPD solution also increased the membrane surface roughness, hydrophilicity and water permeability. The membrane with 0.05 wt/v% silica in MPD solution showed the highest NaCl rejection (89%) with a higher water flux (15 LMH) than that of the unmodified membrane (72% and 10.3 LMH) in AL-FS orientation. The improvement in salt rejection at higher silica loadings was associated with the pore blockage of membranes by silica nanoparticles, which is supposed to reduce the water flux too. On the contrary, integration of silica in PA active layer unexpectedly enhanced water flux. Additionally, the authors attributed the decrease in NaCl rejection (increase in salt flux) observed at the highest silica loading of 0.1% wt/v% (TFN0.1) to the formation of a defective PA layer. A defective selective layer is supposed to increase the salt flux across the membrane as suggested by the authors. However, the FO test results showed that the TFN0.1 demonstrated the lowest salt flux compared to other TFN membranes, which contradicts the results obtained for NaCl rejection in RO test.

2.2 Carbon nanotubes and graphene oxide

CNT-modified membranes have been researched extensively for desalination and water purification due to their low biofouling potential, good chlorine resistance, self-cleaning properties, superior separation and mechanical properties [103-106]. The hollow tubular structures of CNTs act as pores in membranes and facilitates frictionless transport of water molecules to produce high water flux [107]. Besides, the specific pore diameter of CNTs helps to improve the membrane selectivity by rejecting salt ions and permitting transport of water molecules [108]. Owing to the hydrophobicity of CNTs and their inadequate dispersibility in

organic/aqueous monomer solution or polymer matrix, it is required to functionalize CNTs with carboxylic or amine functional groups by treating them with acids or amines. The dispersion of CNTs in polymer dope or monomer solutions for IP reaction can be extensively influenced by the functionalization reaction conditions of CNTs like acid concentration, reaction temperature and time [109].

Rahimpour and co-workers amine-functionalized multi-walled carbon nanotubes (f-MWCNTs) using 1,3-phenylenediamine (mPDA) to augment the hydrophilicity of PA TFC membranes [78, 110]. The CNTs were first carboxylated by treating in a H_2SO_4: HNO_3 mixed acid solution with a volume ratio of 3:1 at 90°C for 1 h. The carboxylated CNTs were then added to mPDA dissolved in dimethylformamide at 70°C for 96 h. The most permeable membrane, with a loading of 0.1 wt% f-MWCNTs (TFN0.1) in MPD aqueous solution, achieved a water flux of 95.7 LMH in AL-DS orientation, which is roughly 160% more than that of TFC membrane [78]. The NaCl rejection for TFN0.1 and the control membrane was observed to be similar (70-73%) and was evaluated using a cross-flow RO setup with 20 mM NaCl feed and a pressure of 2.4 bar. The authors deduced that the enhanced water flux in TFN membranes could have resulted from the capillary force within the f-MWCNTs nanochannels or from the formation of external nanochannels (voids) between the polymer and f-MWCNTs at the PA layer interface. The increased surface hydrophilicity of TFN membranes could have also increased the water permeation through the membrane. The TFN membranes exhibited a lower solute flux than that of the control membrane; however, the authors did not discuss the possible reasons that enhanced membrane selectivity. Kim et al. later reported that the decline in solute flux might be ascribed to the formation of narrower nanochannels due to PA partially covering CNTs, which hindered the transport of hydrated solute ions [109].

Wang and his group were the first to prepare double-skinned TFN membranes using unmodified CNTs [79]. They also explored the impact on membrane performance and

334 characteristics by changing the location of CNTs inside the membrane [83]. In both studies,
335 the membranes were prepared via IP of polydopamine (pDA)/CNTs and TMC on PSf
336 substrates; and the contact angles of TFC and TFN membranes at all conditions were observed
337 to be similar (67.0°-67.5°). This is because the unmodified CNTs did not improve membrane
338 hydrophilicity, unlike the amine-functionalized CNTs prepared by Rahimpour's group (47.4°
339 with 0.05 wt% CNTs in the PA layer) [78]. The double-skinned membranes, both TFC and
340 TFN, were found to exhibit outstanding solute rejection compared to single-skinned
341 membranes without sacrificing water flux. The anti-fouling capacity of the double-skinned
342 membranes to humic acid (HA) was much higher than that of single-skinned membranes. The
343 TFN double-skinned membrane with 0.05 wt% CNTs (TFN0.05) had the highest anti-fouling
344 capacity because CNTs in the active layer weakened the adhesion between CNTs and HA. The
345 normalized flux recovery for double-skinned TFN0.05 was 81.4% after the third cycle of
346 fouling and cleaning process, which was much higher than the double-skinned TFC membrane
347 (60.8%). Moreover, water flux through the TFN0.05 double-skinned membrane was 54%
348 higher than the control double-skinned membrane in AL-FS orientation. In addition,
349 incorporation of CNTs into both the PA active layer and substrate of single-skinned TFC
350 membrane (nTFN) improved membrane porosity, which led to a reduction in the structural
351 parameter. Similar to the double-skinned TFN membranes, nTFN membranes demonstrated
352 enhanced antifouling property to HA. The normalized flux recovery for nTFN membrane was
353 87.8% after the third cycle of fouling and cleaning process, compared to 70.7% flux recovery
354 achieved by the TFC membrane. Although the nTFN membranes demonstrated higher water
355 flux, the CNT-polymer incompatibility resulted in poor salt rejection due to the formation of
356 macrovoids within the polymer matrix.

357 GO is a chemical derivative of graphene with abundant surface functional groups and a
358 high area-to-thickness ratio [111]. GO is amphiphilic and can improve water flux by creating

359 water channels between the GO interlayers, where water molecules are initially adsorbed by
360 the hydrophilic hydroxyl groups and then diffused rapidly between the hydrophobic carbon
361 core [112]. The hydrophilic nature of GO promotes better GO dispersion in water, and assists
362 in the development of nano-sized laminates involving GO layers in forming mesh-like structure
363 [113], which is beneficial for water filtration membranes. GO has been studied only recently
364 for preparation of high-performance polymeric membranes for water treatment applications
365 [114-117]. GO-modified membranes were reported to have better water permeability, salt
366 rejection, mechanical strength, chlorine resistance, surface charge and antimicrobial properties
367 than pristine membranes in various applications like UF, RO and FO [118-122]. GO
368 membranes have also been studied for solvent pervaporation and NF as the membranes are
369 chemically inert [123-126]. Several reviews have been published recently that discuss the
370 application of GO-based membranes in various areas [113, 127, 128].

371 The GO-incorporated PA TFN membrane not only demonstrated enhanced
372 hydrophilicity and surface smoothness but also had a thinner PA layer compared to the control
373 TFC membrane [90]. As a result, water permeability increased upon GO incorporation in PA
374 layer. The optimal GO loading in the PA layer was reported to be about 400-600 ppm, beyond
375 which the performance of TFN membranes aggravated due to GO agglomeration. The water
376 flux achieved in AL-FS orientation with 600 ppm GO-incorporated TFN membrane was ~ 48%
377 higher compared to that of the unmodified membrane with a comparable solute flux. The
378 smooth, hydrophilic and negatively-charged surface of the GO-modified membrane was also
379 able to efficiently suppress sodium alginate (SA) fouling by electrostatic repulsion and
380 providing fewer adhesion sites on the membrane surface. The flux recovery ratio (FRR) value
381 of TFC membranes was only ~60% after cleaning; whereas, the FRR value of all GO-modified
382 membranes was higher than 90% [90].

GO was also chemically modified to improve its dispersibility in MPD aqueous solution and minimize its aggregation in the polymer matrix. Polyvinylpyrrolidone (PVP) coated GO (PVP-GO) was synthesized by Wu et al. as a nanofiller to prepare TFN membrane for desalination [92]. It was found that PVP-GO had better dispersion than unmodified GO in MPD aqueous solution, which helped to reduce GO aggregation in the PA layer. Moreover, the membrane hydrophilicity, salt rejection and water flux of PVP-GO modified membranes were much higher than pristine TFC and unmodified-GO-incorporated TFN membranes. The optimal TFN membrane with a PVP-GO loading of 0.0175 wt% demonstrated a water flux of 33.2 LMH in AL-DS orientation, which is approximately 3.3 times greater than that of pristine TFC membrane when 10 mM and 2 M NaCl feed and draw solution, respectively.

2.3 Other carbon-based nanomaterials

Graphene quantum dots (GQDs) have been recently studied as biocidal agents in TFC FO membranes by Seyedpour et al. [99]. The oxygen-containing functional groups on the surfaces of GQDs allows them to demonstrate excellent water solubility and polymeric compatibility. The biocidal property of GQDs occurs from their electron transport property, which improves their peroxidase activity. Incorporation of 0.5 wt% GQD in the MPD solution during IP reaction, not only improved the TFN FO membrane's anti-bacterial property (>90% and 95% inactivation for E. coli and S. aureus, respectively during 1h incubation), but also enhanced FO performance by increasing membrane surface hydrophilicity. Additionally, the strong covalent bonding between the GQDs and PA layer ensured long-term membrane stability during FO test. The authors attributed the exceptional anti-bacterial property of GQD-modified TFC FO membrane to the uniform dispersion of GQDs that enabled more of their active edges to disrupt bacterial cells on the membrane surface via contact mechanism. Nonetheless, the contact mechanism for cell disruption is unlikely to be effective when GQDs are embedded in the polymer matrix as suggested by Faria et al. [129]. This is because, most

of the nanoparticles are washed off with the excess monomer solution during the IP process, and the remaining nanoparticles on the substrate surface get embedded in the PA layer. However, there are other studies, which reported that graphene derivatives could kill bacteria by contact mechanism even when embedded in the PA layer [130, 131]. Hence, the exact mechanism behind the antimicrobial property of graphene derivatives when embedded in a polymer matrix is still dubious and should be further investigated.

Fullerenols are carbon-containing spherical molecules ($C_{60}(OH)_n$) with abundant hydroxyl groups, which have also been used to modify the PA layer to augment the hydrophilicity and antifouling properties of the TFC FO membranes. Recently, Perera et al. developed fullerenol-modified TFC membrane, and a 400 ppm fullerenol loading (FTFC-4) demonstrated a 83% increase (26.1 LMH) and 78% decrease (0.18 g/L) in the water flux and specific reverse solute flux (SRSF), respectively, compared to those of the TFC membrane when tested in AL-FS orientation using DI water as feed solution against 1 M NaCl as draw solution [97]. Although this study attributed the improvement in water flux of the fullerenol-modified TFC membranes to the increased membrane surface hydrophilicity, no in-depth explanation has been provided for their improved selectivity. Moreover, the authors stated that incorporation of fullerenol creates interfacial voids between the fullerenol and the PA matrix that facilitate quick transport of water molecules. In that case, the solute flux is also expected to increase at higher fullerenol loadings as interfacial voids are mostly non-selective and allow draw solutes to diffuse across the membrane easily. However, the salt flux was observed to decrease up to a fullerenol loading of 400 ppm. A change in surface charge of the nanocomposite membranes could have increased salt rejection, but no such data was provided by the authors for further validation. Besides good membrane performance, FTFC-4 demonstrated good antifouling propensity by acquiring a FRR value of 87.2%, which is significantly higher than the FRR value of TFC membrane (53.4%). The hydrophilic surface

433 of the fullerenol-modified TFC membrane created a hydration layer that hindered the progress
434 of foulant adsorption on the membrane surface and created a loose cake layer that could be
435 easily eradicated by physical cleaning [97].

436 *2.4 Titanate and halloysite nanotubes*

437 Besides CNTs, titanate nanotubes (TNTs) and halloysite nanotubes (HNTs) have also
438 been explored as nanofillers for fabricating TFN FO membranes because their tubular form
439 provides additional channels for water transport across the membranes. Both TNTs and HNTs
440 have hydrophilic properties, good stability, and large pore volumes and specific surface area
441 [132, 133]. Although TNTs, HNTs and CNTs have similar tubular and hydrophilic
442 characteristics, the cost of production for HNTs and TNTs is significantly lower than that of
443 CNTs [134, 135].

444 To date, only a few scientific articles have been published on TNTs and HNTs-modified
445 FO membranes; most of which have been produced by Ismail's group [80-82, 136, 137]. The
446 first and only study exploring the possibility of self-synthesized amine-functionalized TNTs as
447 nanofillers for TFN FO membrane was reported by Emadzadeh et al. in 2015 [80]. The surface
448 of calcinated hydrophilic TNTs was amine-functionalized using 1-(2-amino-ethyl)-3-
449 aminopropyl] trimethoxysilane (AAPTS) to prevent agglomeration OF TNTs in the PA active
450 layer during the IP reaction. The amine-functionalized TNTs (f-TNTs) dispersed in the
451 TMC/cyclohexane solution were covalently bonded to the PA layer by forming amide linkages
452 during the IP reaction as shown in Figure 4. The f-TNT modified membranes had higher surface
453 roughness and hydrophilicity compared to the control TFC membrane. As a result, the water
454 flux of the TFN membrane with 0.05 wt% f-TNT loading was 2 times more than that of the
455 control membrane in both membrane orientations. Additionally, the nanochannels of f-TNTs
456 and voids between f-TNTs and PA matrix may have also contributed to the increased flux of

457 the TFN membranes. The authors believe that f-TNTs assisted in a higher degree of PA cross-
458 linking by facilitating quick MPD diffusion to the surface of hydrophilic f-TNTs. The high PA
459 cross-linking degree in TFN membrane resulted in lower reverse solute flux for TFN
460 membranes in both orientations than the control membrane.

461

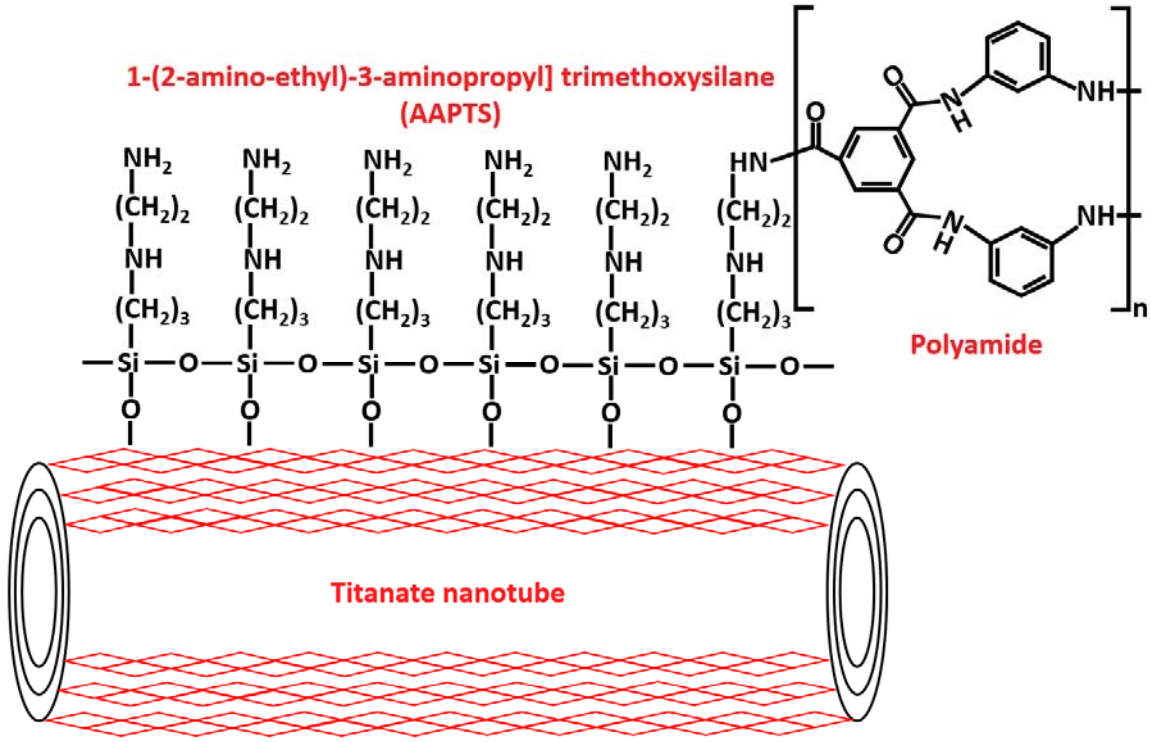

462

463 Figure 4: Schematic illustration of the interaction between amine-functionalized titanate nanotube and polyamide
464 (adapted from [80]).

465

466 Besides incorporating only one type of nanofiller in the PA layer, two or more nanofillers
467 have occasionally been embedded in the TFN membrane to improve FO membrane
468 performance. For instance, Ghanbari et al. investigated the effect of adding HNTs [81] and
469 TiO_2-coated HNTs (TiO_2/HNT) [82] in the PA layer on the performance and anti-fouling
470 property of the membranes. The experimental results showed that compared to HNTs, the

degree of TiO_2/HNTs aggregation in the active layer was negligible due to their good compatibility with PA structure. Moreover, integration of TiO_2/HNTs into PA active layer enhanced membrane hydrophilicity, which resulted in better separation performance compared to pristine TFC and HNTs-incorporated TFN membranes. The 0.05 wt% TiO_2/HNT incorporated TFN membrane, demonstrated a water and solute flux of 40.8 LMH and 7.3 gMH, respectively with 2 M NaCl as draw solution and 10 mM NaCl as feed solution in AL-DS mode. Whereas, the TFN membrane with 0.05 wt% HNTs (TFC membrane) attained a water flux of 33.6 LMH (24 LMH) and a solute flux of 9.2 gMH (6.4 gMH). The tubular structure of HNTs provided additional passages for water molecule transport across the membranes. The TiO_2/HNTs nanoparticles also significantly enhanced the anti-fouling property of the TFN membranes to bovine serum albumin (BSA). The normalized flux of TFC membrane decreased to 0.71 after 10 hours of fouling test; while, the normalized flux decreased to ~0.88 and 0.85 for TiO_2/HNTs and HNTs TFN membrane respectively. The BSA fouling in TiO_2/HNTs and HNTs-modified TFN membranes was almost entirely reversible with a water recovery of 100% and 96.5%, respectively compared to a recovery of ~83% with TFC membrane. The improved hydrophilicity of the TFN membranes enhanced their anti-fouling property by weakening the interactions between the BSA foulant and PA layer.

2.5 Porous coordination polymers

In recent years, porous coordination polymer (PCP), a new kind of nanomaterial, has been used to develop nanocomposite membranes for various applications like gas separation, liquid separation and catalysis [138-144]. Metal-organic frameworks (MOFs) and covalent-organic frameworks (COFs) are two or three-dimensional PCPs, which have been used to improve the structure and performance of FO nanocomposite membranes [85, 86, 88, 145, 146]. MOFs are porous inorganic/organic hybrid nanostructure material comprising of metal ions coordinated to organic ligands as linkers [147, 148]; whereas, COFs are organic

nanoporous solids with extended structures of light elements comprising functional groups that are linked by strong covalent bonds [149].

MOFs and COFs are promising for membrane application as their pore structure can be customized, and they have an exceptionally high surface area, porosity and thermal stability. Moreover, the existence of organic linkers in MOF and COF assembly improves their compatibility with the polymer matrix compared to inorganic nanofillers, which minimizes the development of non-selective cavities between the MOFs/COFs and the polymer matrix. The formation of covalent or non-covalent bonds between MOFs/COFs and polymer could attribute to their good compatibility in the polymer matrix, which can be beneficial for enhancing the properties of the PA layer without compromising on the membrane selectivity [150].

Ma et al. modified the PA layer using self-synthesized zirconium (IV) carboxylate MOFs (UiO-66) to produce highly selective TFN FO membranes [85]. The hydrophilicity and molecular-sieving effect of UiO-66 increased the water permeability of the TFN membrane by 52% (0.1 wt% UiO-66 loading) compared to the control TFC membrane. As a consequence of the hydrophilic nature of UiO-66, increasing its concentration in the organic phase also increased the PA layer thickness. Increasing the UiO-66 loading beyond 0.1 wt% formed a very thick PA layer, which decreased water flux by increasing the transport resistance of the water molecules in the active layer. The TFN membrane with 0.1 wt% UiO-66 loading showed a 40% (AL-DS) and 25% (AL-FS) increase in water flux than the control TFC membrane without significantly affecting the membrane selectivity.

Similarly, Zirehpour et al. found that dispersing MOFs, consisting of silver (I) and 1,3,5-benzene tricarboxylic acid (3HBTC), in the PA layer of FO membranes improved both the membrane hydrophilicity and transport properties without negatively altering the membrane selectivity for seawater desalination [86]. With an optimal MOF loading of 0.04 wt/v%, the

water flux of TFN0.04 increased by 27% compared to the TFC membrane without deteriorating membrane selectivity. However, the integrity of the PA layer was lost when MOF loading was increased beyond 0.04 wt/v%, which hampered membrane selectivity.

The first study that investigated the effect of COF nanofillers, Schiff base network-1 (SNW-1), on the performance of PA TFN membrane for FO process was conducted by Akther et al. [88]. The hydrophilic SNW-1 nanoparticles reacted with the acyl chloride groups of TMC during the IP reaction to form strong tertiary amide bonds, which aided the stability of SNW-1 nanoparticles in the PA layer. Addition of SNW-1 nanoparticles formed a thinner PA layer by hindering the reaction between MPD and TMC during the IP reaction. The thin PA active layer reduced the transport resistance and the porous SNW-1 structure provided extra channels for water molecule transport. As a result, the TFN membranes demonstrated higher water flux than the pristine TFC membrane. The optimal SNW-1 loading was found to be 0.005 wt% (TFN0.005), which increased the water flux by 29% from that of the control membrane when tested in AL-FS orientation with deionized water and 0.5 M NaCl as feed and draw solution, respectively.

2.6 Issues and challenges of nanomaterial-modified PA layers

The selectivity of TFC membranes depends on the integrity of their dense PA layer, which will be affected upon addition of nanomaterial. Nanoparticle incorporation in the PA active layer mostly improves water permeability but at the expense of membrane selectivity. The performance of TFN membranes that are able to overcome the trade-off relationship is only marginally better than those of pristine TFC membranes. Any further increase in nanoparticle loading can cause particle agglomeration and hinder the reaction between monomers during the IP process. As a result, a defective PA layer will form that will reduce membrane selectivity. Moreover, the effective nanoparticle loading in the PA layer is much lower than that in the monomer solution as most of the nanoparticles are washed out when extra monomer solutions are discarded during the IP process. Consequently, a significant quantity of nanomaterial is lost, which can make the commercial development of TFN membrane costly.

One possible strategy to reduce nanomaterial loss during the fabrication process is to use a vacuum-assisted IP process [151, 152]. Additionally, nanoparticles may be lost during FO operation if they are incompatible with the PA matrix. Therefore, fabrication techniques should be improved, and polymer-compatible nanoparticles should be developed to achieve cost-effective development of TFN membranes. This may include exploring new nanomaterials or modifying the existing commercially available nanomaterials through functionalization to enhance their stability within the PA matrix.

3. Nanomaterial-coated PA layer surfaces

Surface modification is an attractive technique as it allows alteration of membrane performance without significantly changing the intrinsic structures of the membrane. Surface modification allows nanomaterials to be directly coated, grafted, assembled by a layer-by-layer (LbL) method or covalently bonded to the TFC membrane surface. Modification of membrane surface using nanoparticles is often adopted to improve membrane hydrophilicity, tune the charge density and surface roughness in order to reduce membrane fouling, impart biocidal properties, enhance chlorine resistance, and eliminate the trade-off between membrane selectivity and water permeability. For instance, Yang et al. stacked GO nanosheets on membrane supports to enhance selectivity and anti-fouling property of the membranes [153, 154]. Table 3 presents the studies on surface modified TFC FO membranes.

565 Table 3: Summary of the fabrication conditions and FO performance of PA TFC membranes with nanomaterial-modified surfaces

TFC membrane surface modification using nanomaterials		Modification method	Modification benefits	FO performance (AL-FS)				Year (Ref)
Nanomaterial or nanocomposite (Particle size)	Substrate (PA layer monomers)			DS (FS)	CFV	Jw (LMH)	Js (gMH)	
f-SWNTs (n/a)	PSf (MPD, TMC)	EDC/NHS facilitated GO binding	Improved hydrophilicity Biofouling control	-	-	-	-	2011 [47]
Superhydrophilic ligand-coated SiO_2 nanoparticles (D: ~8 nm)	PSf (MPD, TMC)	Dip-coating	Reduced surface roughness Improved hydrophilicity Lower fouling propensity: hydration layer barrier	-	-	-	-	2012 [155, 156]
Ag-PEGylated dendrimer (n/a)	PES (MPD, TMC)	In situ synthesis of AgNPs via photolysis of $AgNO_3$ within the PEGylated dendrimer matrix	Antiadhesive and antibacterial properties Anti-protein fouling property	1 M NaCl (DI water)	3.3 cm/s	25.0	5.0	2013 [157]
GO/PLL (n/a)	PSf (MPD, TMC)	EDC/NHS facilitated GO/PLL grafting	Improved hydrophilicity and selectivity Anti-biofouling and biocidal property	2 M NaCl (DI water)	500 mL/min	11.0	15.0	2015 [158]
GO-Ag (n/a)	PSf (MPD, TMC)	In situ synthesis of AgNPs on GO surface by chemically reducing $AgNO_3$. GO-Ag nanocomposites grafted onto the membrane surface via amide forming condensation reaction	Improved hydrophilicity Antibacterial properties	1 M NaCl (DI water)	200 mL/min	5.4	35.1	2015 [44]
$BaSO_4$ (n/a)	PSf (MPD, TMC)	Deposition of $BaSO_4$ via surface mineralization of TFC membrane with $BaCl_2$ and Na_2SO_4 aqueous solutions using ASP technique	Improved surface hydrophilicity Better FO performance	1 M NaCl (DI water)	250 mL/min	10.7	3.99	2015 [159]
GO (T: ~1.4 nm, A: 0.19 μm^2)	PSf (MPD, TMC)	EDC/NHS facilitated GO binding	Improved hydrophilicity Antiadhesive and antimicrobial properties Biofouling resistance	-	-	-	-	2014 [160] 2016 [131]
GO-pDA	PSf	Coating	Smoother membrane surface	2 M NaCl	500	13.0	8.75	2016

(T: 1.5-2.5 nm, Lateral size: 0.2-1 μm)	(MPD, TMC)		Improved hydrophilicity Biofouling resistance	(DI water)	mL/min			[48]
Ag (n/a)	PSf (MPD, TMC)	In situ production of AgNPs on GO-modified membrane surface via wet chemical reduction of $AgNO_3$ by $NaBH_4$	Improved antibacterial property 98% bacterial inactivation with E. coli	-	-	-	-	2016 [161]
AgCl (n/a)	PSf (MPD, TMC)	Deposition of AgCl via surface mineralization of TFC membrane with $AgNO_3$ and NaCl aqueous solutions using ASP technique	Improved surface hydrophilicity Better FO performance Fouling resistance Better phenol removal efficiency	1 M NaCl (DI water)	315 mL/min	24.0	2.8	2017 [162] 2018 [163]
Ag (28.1 nm)	PSf (MPD, TMC)	In situ synthesis of AgNPs on pDA-coated TFC membranes by incubation in $AgNO_3$ aqueous solution at room temperature for 2 h	Improved anti-adhesive and anti-bacterial property 94% reduction in cell viability with P. aeruginosa	-	-	-	-	2018 [164]
Zwitterion-Ag (n/a)	PES (MPD, TMC)	In situ formation of AgNPs via reduction of Ag^+ using 0.01M $NaBH_4$	Antiadhesive and antibacterial properties >96% antimicrobial efficiency with E. coli	1 M NaCl (DI water)	8.5 cm/s	15.2	7.7	2018 [165]

AgCl: silver chloride; $AgNO_3$: silver nitrate; AgNP: silver nanoparticle; ASP: alternate soaking process; BaCl: barium chloride; $BaSO_4$: barium sulfate; CFV: cross-flow velocity; DS: draw solution; EDC: *n*-(3-Dimethylaminopropyl)-*n'*-ethylcarbodiimide hydrochloride; FS: feed solution; *f*-SWNTs: functionalized single-walled carbon nanotubes; GO: graphene oxide; Js: solute flux; Jw: water flux; MPD: m-phenylenediamine; $NaBH_4$: sodium borohydride; NaCl: sodium chloride; Na_2SO_4: sodium sulfate; NHS: *n*-hydroxysuccinimide; pDA: polydopamine; PEG: polyethylene glycol; PES: polyether sulfone; PLL: poly-L-lysine; PSf: polysulfone; SiO_2: silica; TMC: trimesoyl chloride

3.1 Carbon nanotubes and graphene oxide

Tiraferri et al. developed membranes with biocidal properties by covalently binding antimicrobial functionalized single-walled CNTs to the TFC membrane surface using amide bonds. Based on characterization results, it was observed that the CNTs were firmly bonded to the surface of the membrane and provided a homogenous surface coverage. The modified membrane was able to inactivate up to 60% of the bacteria adhered to membrane surface within an hour of contact time; thus, indicating its potential to delay initiation of membrane fouling during FO process [47]. The same research group also altered the surface chemistry of the TFC membrane using modified silica nanoparticles to achieve lower foulant-membrane adhesion for fouling mitigation. The surface of the silica nanoparticles was altered via super hydrophilic ligands coating that made the silica nanoparticles more stable and bind irreversibly to the carboxylic groups of the PA layer using the dip-coating technique. Although the surface chemistry of the TFC membrane changed due to nanoparticle coating, the morphology and salt/water permeability of the membrane remained the same as that of the pristine membrane. The uniform coating of nanoparticles on the membrane surface increased the surface hydrophilicity, which formed a tightly bound hydration layer on the membrane surface. The hydration layer acted as a barrier between the membrane and the organic foulants. The neutralization of membrane carboxyl groups also contributed to the membrane's anti-fouling property [155, 156].

Surface coating of the membrane using biocidal GO nanosheets is often challenging. To overcome this issue, Hegab et al. utilized bioadhesive pDA to incorporate GO nanosheets on the TFC membrane surface. Deposition of pDA takes place via oxidative polymerization and self-assembly, both of which reduce and immobilize GO on the membrane surface. The best performing GO-pDA membrane was fabricated using a GO concentration of 80 μg/mL and pDA deposition time of 30 min. At the optimal GO loading, the GO nanosheets did not

aggregate and bound firmly to the membrane surface. The optimal GO-pDA modified membrane demonstrated 21.5% and 80% higher water flux and selectivity, respectively compared to the pristine membrane because of improved membrane hydrophilicity and morphology. Moreover, the modified membrane was able to significantly extend the biofouling onset because of its outstanding anti-bacterial properties [48].

Perreault et al. investigated the anti-biofouling property of GO by covalently bonding GO nanosheets on commercial TFC FO membranes using amide coupling reaction. In addition to possessing improved antimicrobial property, the GO functionalized TFC membrane demonstrated enhanced surface hydrophilicity without significantly affecting its transport properties. During the treatment of synthetic secondary wastewater accompanied with P. aeruginosa cells, the GO functionalized membranes showed a flux decline of 20% after 24 h of operation due to biofouling; whereas, a 40% flux decline was observed with the unmodified membrane. The improved anti-bacterial property of the GO modified membrane can be ascribed to the reduction of microbial biomass build-up on the membrane surface owing to the biocidal property of GO nanosheets [131].

Hegab et al. used two unique techniques, layer-by-layer (LbL) and hybrid (H) grafting, to covalently attach GO nanosheets on the PA TFC membrane surface through a poly L-Lysine (PLL) intermediary. The GO nanosheets were firmly bound to the membrane surface and each other when hybrid grafting technique was used, which resulted in better membrane hydrophilicity, morphology, smoother surface and antibacterial property. The GO/PLL-H membrane demonstrated higher selectivity compared to the pristine and GO/PLL-LbL membranes due to the formation of a tight active layer. The GO/PLL-H and GO/PLL-LbL membranes reduced the bacteria by 99% and 48.5%, respectively, compared to the pristine membrane. GO nanosheets enhanced the anti-bacterial properties of the membranes by penetrating and damaging the bacterial cell membranes with their sharp edges. Additionally,

when PLL bonded GO nanosheets pierced the bacterial cell membranes, they inhibited several cellular enzymatic systems that killed the bacteria and impeded bacterial growth. The reverse solute flux demonstrated by GO/PLL-LbL membrane was 78% higher than the pristine membrane because of substantial swelling that occurred as a result of membrane coming in contact with high salt concentration and forming loose structures that increased both ICP and draw solute diffusion [158].

Besides modifying membranes for use in water treatment processes, the surface of the PA layer was impregnated with nanomaterials for rejection or adsorption of trace pharmaceuticals [166] and shale gas wastewater treatment [167]. The modified TFC membrane demonstrated less fouling tendency and higher rejection capacity for pharmaceuticals than the pristine membrane. In the case of shale gas water treatment, a membrane comprising of a GO-incorporated PES substrate and a salt-rejecting and oil-repelling hydrogel selective layer was used. The modified membrane exhibited excellent fouling resistance under several oil/water emulsions due to the robust underwater oleophobicity of the hydrogel selective layer. The structural parameter of the GO-incorporated support was 20% lower than the virgin membrane. The membrane also demonstrated 3 times higher water flux than the commercial FO membrane and removal percentage higher than 99.7% and 99.9% for multivalent ions and oil, respectively.

3.2 Silver nanoparticles and nanocomposites

Chung and co-workers coated TFC membrane surface with silver–polyethylene glycol PEGylated dendrimer nanocomposite to diminish both protein and bacterial fouling that occur during water treatment processes. They compared the anti-fouling property of four types of functional groups (carboxylic acid, amine, PEG or silver nanoparticles) that were imparted on the TFC membrane surface during the modification process (Figure 5). All modified membranes obtained desired electrochemical characteristics and demonstrated enhanced

hydrophilicity and anti-fouling property compared to the pristine membrane. However, the silver–PEGylated dendrimer modified membrane was the most effective in fouling mitigation and decreased fouling by 99.8%. The silver nanoparticle and PEG-modified membranes weakened the electrostatic interactions between the membrane surface and the foulants to lower the protein fouling propensity. Whereas, the strong electrostatic interactions between the amine-modified membranes and the proteins resulted in quick initial protein deposition on the membrane surface [157].

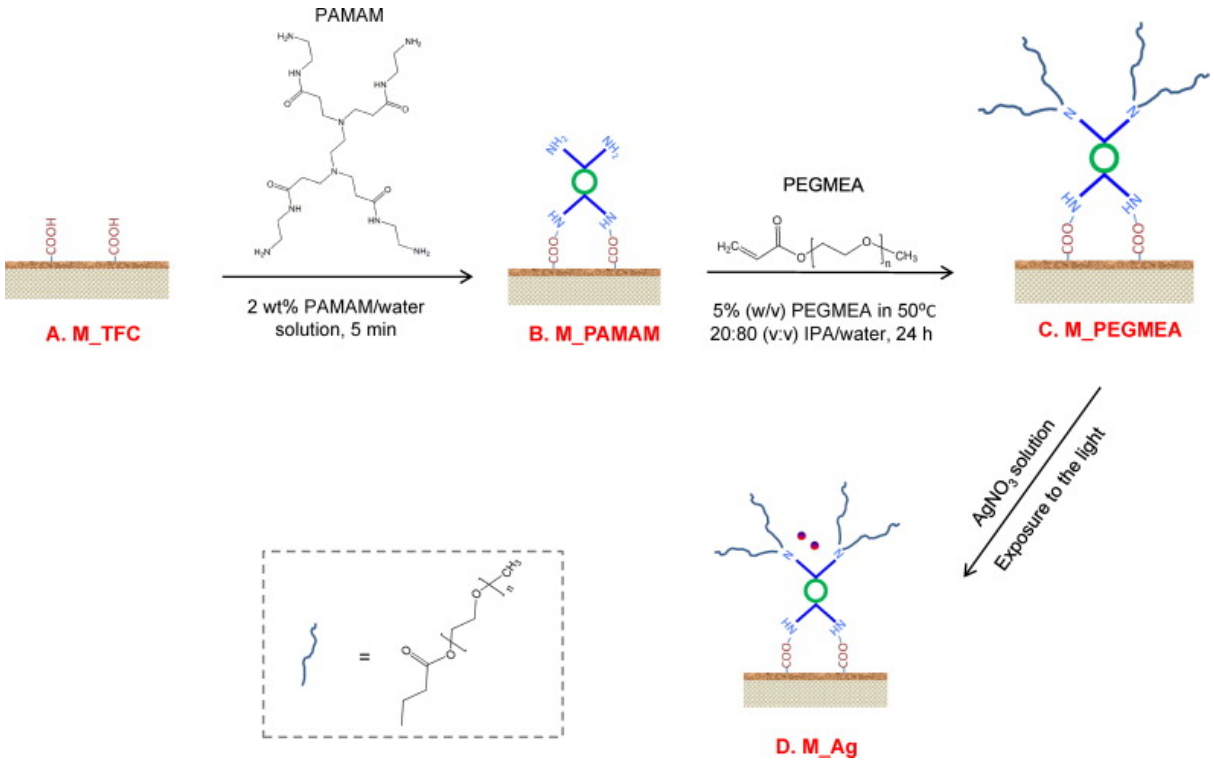

Figure 5: Illustration of the steps involved in the modification of PA TFC membrane surface with silver–PEGylated dendrimer nanocomposite structure [157].

Qiu and He developed a zwitterion-Ag nanocomposite to increase the biofouling resistance and water flux of the TFC FO membrane without significantly deteriorating the membrane selectivity [165]. The nanocomposites were assembled on the membrane surface using a second

IP of zwitterion followed by in situ preparation of silver nanoparticles (AgNPs). The carboxylic acid functional groups of zwitterions acted as binders to Ag ions and reduced them to AgNPs. The hydrophilic and functional surface of the modified membrane resulted in better water flux and selectivity compared to the unmodified TFC membrane. The zwitterion-Ag nanocomposite improved the membrane biofouling resistance by improving the anti-adhesion and anti-bacterial property of the membranes. The modified membranes also demonstrated long-term biofouling resistance with an antimicrobial efficiency greater than 96%. A flux decline of only 8% was observed with the modified membrane after 10 hours of fouling test; whereas, a 50% flux decline occurred with the unmodified membrane. Additionally, it was possible to regenerate the AgNPs on the membrane surface once it was used up [165].

Silver nanoparticles (AgNPs) have also been studied as a biocidal agent by Soroush et al. where silver nitrate was reduced to AgNPs via wet chemical reduction on the surface of GO nanosheets to form silver-coated GO (GO/Ag) nanocomposites [44]. GO was chosen as a substrate to reduce the agglomeration of AgNPs. Moreover, GO offered a larger active surface area to AgNPs by dictating spherical morphology, which resulted in higher antimicrobial activity. The GO/Ag nanocomposites were bonded covalently to the surface of the PA layer via amide forming condensation reaction using cysteamine via dip-coating technique. Surface modification improved the hydrophilicity of membranes and inactivated bacteria (*E. coli*) by more than 95% without significantly changing the membrane transport properties. The antibacterial property of the membranes modified with GO/Ag nanocomposites was found to be much more effective than using GO (40%) or silver nanoparticles (60%) individually due to the synergistic capture-killing mechanism exhibited by the GO/Ag nanocomposites. GO/Ag nanocomposites inactivate bacteria by (1) penetrating silver ions into the bacterial cells, (2) capturing bacteria onto the GO surface, (3) and breaking the bacterial membrane through the sharp edges of GO nanosheets.

In addition to exploring the biocidal properties of GO/Ag nanocomposites, Soroush et al. modified commercial HTI TFC FO membranes via in situ development of AgNPs on both the control and GO-modified TFC membrane surfaces. The GO-incorporated membrane surface resulted in a more uniform AgNPs distribution and production of smaller sized AgNPs due to the presence of oxygen-containing functional groups on the GO surface. The functional groups on the surface of GO also provided better anchoring to silver ions that facilitated improved stability, higher Ag loading and greater control on Ag ion release. In terms of biocidal properties, GO/Ag modified FO membranes demonstrated higher bacterial inactivation (98%) than the Ag-only modified (80%) or GO-only modified membranes (50%). Regeneration of AgNPs on the GO/Ag modified membrane surface after 7 days of Ag leaching resulted in the retrieval of 70% of the initial silver loading, and almost complete restoration of its antibacterial properties (95%) [161].

The antibacterial property of AgNPs was further investigated by combining pDA and AgNPs to simultaneously achieve both passive and active antibacterial properties [164]. Under static conditions, the pDA coating demonstrated both anti-bacterial and anti-adhesive properties by deactivating 30% Pseudomonas aeruginosa cells and decreasing the number of adhered cells by 85% compared to the control TFC membrane. The pDA coating demonstrated good anti-adhesive property due to the formation of the hydration layer that helped to minimize adsorption of foulants. The anti-bacterial property of pDA coating was ascribed to the protonation of pDA amine groups that assisted in bacteria lysis via contact with the bacterial cell walls. However, the pDA coating failed to prevent the growth of attached cells in dynamic conditions as the experimental conditions increased foulant interaction that covered the membrane surface entirely with biofilm. On the other hand, the AgNPs minimized microbial biomass and inhibited biofilm growth via inactivation of the attached bacterial cells. Moreover, the AgNPs on the TFC FO membrane surface showed good activity and stability during the 24

711 h cross-flow FO operation with a permeate flux decline of only 0.5%. Overall, the authors
712 concluded that the hydrophilic pDA coating would be ineffective in mitigating biofilm growth
713 and biofouling, but its anti-adhesion properties may facilitate easy biofilm removal using
714 physical backwash [164]. Despite several studies proving the regeneration possibility of
715 AgNPs on the membrane surface and its excellent biocidal property, the concern for AgNPs
716 leaching and its effect on the environment cannot be overlooked. Moreover, in situ regeneration
717 of AgNPs on membrane surface requires more chemicals, which is associated with additional
718 costs and negative impacts on the environment.

719 *3.3 Membrane surface mineralization*

720 Besides surface coating and covalent binding, Yu's group adopted a new technique called
721 surface mineralization to chemically-modify membrane surface. Barium sulfate was deposited
722 on PA TFC membrane surface using alternate soaking process (ASP), where the membrane
723 was soaked separately into barium chloride and sodium sulfate aqueous solutions (Figure 6).
724 The number of ASP cycles was varied to prepare membranes with various degrees of
725 mineralization. The characterization results showed that the barium sulfate particles were
726 dispersed uniformly on the membrane surface. The mineral coating did not increase the TFC
727 membrane active layer thickness, but it made the membrane surface smoother and denser.
728 Increasing the mineralization degree made the membrane more negatively charged and
729 hydrophilic. The salt rejection and water flux of mineralized TFC membrane were found to be
730 better than those of the unmodified TFC membrane and commercial CTA FO membrane. The
731 FO water flux of mineralized membrane improved with increasing number of ASP cycles
732 because the enhanced surface hydrophilicity at higher mineralization degree counterweighed
733 the decrease in water permeability caused by the additional barium sulfate coating layer.
734 Increasing the number of ASP cycles also decreased the reverse solute flux as the membrane
735 surface acquired more negative charge, which increased the repulsion force between the

membrane surface and anions (chloride ions) in the draw solution; thus, hindering the permeation of anions across the mineralized membrane [159].

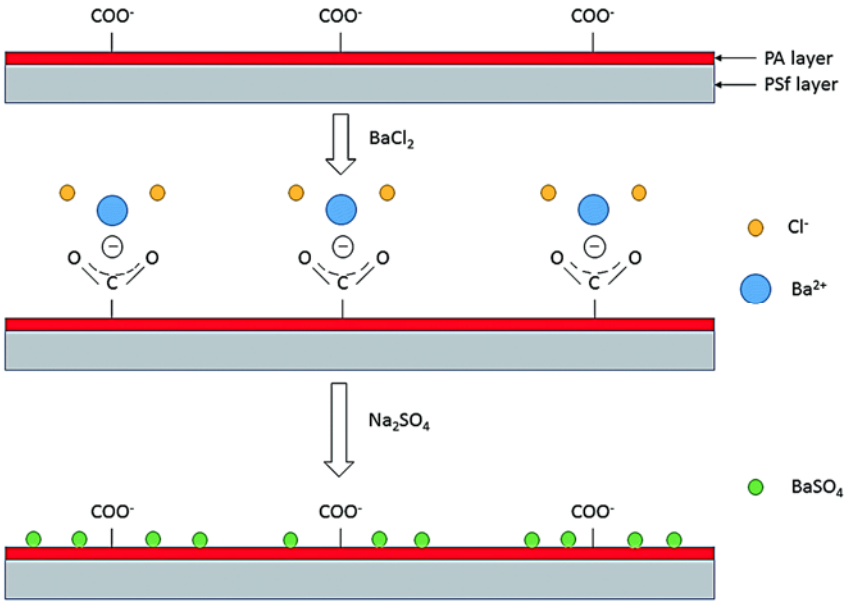

Figure 6: Key steps involved in a single cycle of the alternate soaking process (ASP) for the deposition and coating of barium sulfate on the PA TFC membrane surface [159].

Yu and co-workers also deposited silver chloride on PA TFC membrane surface by separately soaking the membrane in 0.1 M sodium chloride and 0.1 M silver nitrate aqueous solutions using the ASP technique [162]. The membrane fabricated with four ASP cycles (M4) was found to be optimal with a 67.8% higher water flux and 64.5% lower reverse solute flux than the control TFC membrane. The water flux decreased for membranes beyond four ASP cycles (M5 and M6) due to the increased resistance from the large quantity of deposited silver chloride coating. However, all the mineralized membranes demonstrated a higher water flux and lower reverse solute flux than the pristine membrane due to the negatively-charged surface of the mineralized membrane that repelled chloride ions. Additionally, the enhanced surface hydrophilicity of mineralized membranes contributed to lower solute flux by preferentially

allowing water molecules to diffuse through the membrane instead of salt ions. The negative surface charge, reduced surface roughness and improved hydrophilicity of the mineralized membranes enhanced their water flux recovery and fouling resistance to BSA [162]. Due to the high selectivity and improved fouling resistance, the optimal mineralized membrane with 4 ASP cycles was used for separating phenol from water using the FO process. FO performance tests showed higher flux and phenol rejection with mineralized membranes compared to TFC membranes. Moreover, increasing both the feed solution pH and draw solution concentration resulted in better phenol rejection. Maximum phenol rejection of 98.8% was achieved when the feed solution pH was changed to 11. This is because of the electrostatic repulsion existing between the membrane surface and phenolate ion when the feed solution pH is maintained above 9.96, which is the pK_a of phenol. In addition, the phenol adsorption behavior on the membrane surface was found to be significantly influenced by operating parameters and the reverse salt flux, electrostatic interaction and solute hydrophobic character. It was observed from the fouling tests that the phenol fouling for the mineralized membrane was reversible (90% flux recovery of the initial flux) and could be simply eliminated using physical cleaning [163].

Although several studies have considered surface modification of PA TFC membranes, none of them reported the effect of long-term FO operation and nanomaterials leaching on the FO performance. Therefore, investigating the stability of nanomaterials in water and the PA layer is essential to retain a stable FO performance for an extended period. In general, the continuing research on surface modifications of the membrane using nanoparticles has the potential to develop high-performance PA TFC FO membranes with good antifouling properties and chlorine resistance.

3.4 Issues and challenges of nanomaterial-coated PA layer surfaces

Surface modifications with nanomaterials have proven to be successful in imparting chemical functionality and improving the fouling and chlorine resistance of the membranes [168]. However, nanoparticle deposition on membrane surface increases mass transfer resistance and may block pores on the selective layer, which ultimately increases CP and reduces water flux. Therefore, coating layers should be ultrathin to reduce water transport resistance. Advanced surface modification techniques like layer-by-layer (LbL) assembly and chemical vapor deposition (CVD) can be employed as they provide control over coating layer thickness at the nanoscale level. Moreover, the coating layers prepared by the LbL and CVD methods are thinner and more stable than those developed using other techniques [169].

Nanomaterial detachment from the membrane surface is another major issue that occurs with the implementation of physical surface coating methods. Nanomaterial loss will not only reduce membrane functionality but will also cause secondary environmental pollution. For instance, *in situ* formation of silver nanoparticles allows the release of silver ions, which are toxic to both bacterial and human cells [161]. Hence, good mechanical and chemical stability of coating layers is imperative for long term operations, which may be achieved by chemical grafting. Future studies on surface modifications should validate long-term efficiency and stability of the coating layer on the membrane surface under practical conditions.

4. Nanomaterial-modified substrates

A desired PA TFC membrane is anticipated to have not only a dense active layer with high selectivity and water permeability but also a hydrophilic substrate/support with a low structural parameter to minimize ICP and allow a high mass transfer. One possible strategy to achieve high-performance membrane substrates with good mechanical strength, chemical stability and antifouling resistance is to blend nanomaterials in the polymer dope solution. Until now, hollow fiber and flat sheet substrates for PA TFC FO membranes have been produced mostly by phase inversion method as illustrated in Figure 7, and most recently by electrospinning (nanofiber mat). Table 4 and Table 5 summarise the studies on nanomaterial-incorporated TFC FO membrane substrates along with their FO performance.

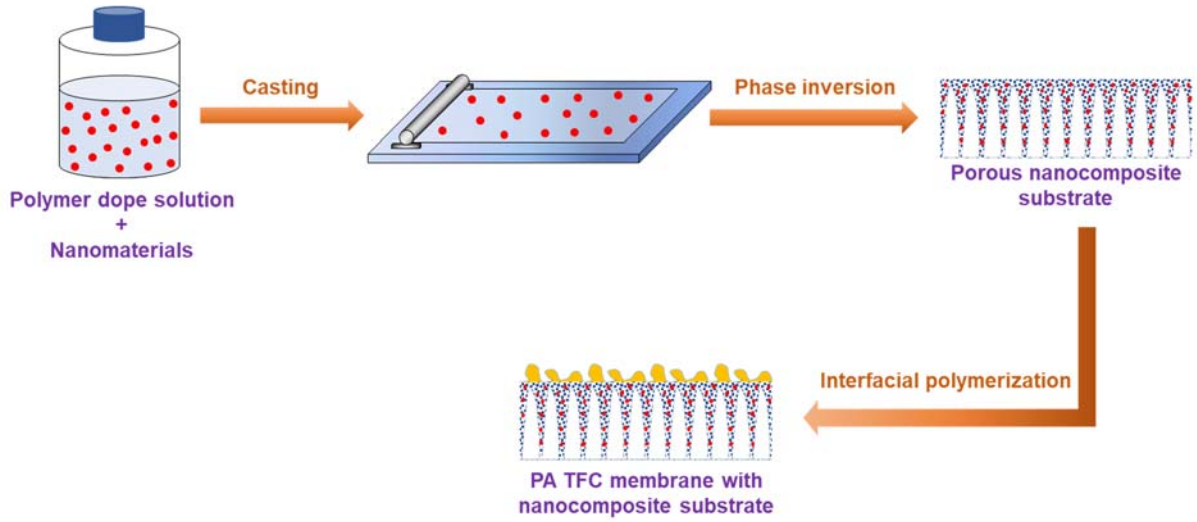

804

805 Figure 7: Typical steps involved in the preparation of a PA TFC membrane with nanomaterial-incorporated
806 substrate.

807 Table 4: Summary of the fabrication conditions and FO performance of PA TFC membranes with porous nanomaterial-incorporated substrates.

TFC membrane with nanocomposite substrate		Optimal particle loading	Intrinsic properties	Substrate fabrication method & conditions	FO performance (AL-FS)				Year [Ref]
Filler embedded in substrate (Particle size)	Substrate (PA layer monomers)				DS (FS)	CFV	Jw (LMH)	Js (gMH)	
Zeolite: NaY (40-150 nm)	PSf (MPD, TMC)	0.5 wt% in dope solution	A = 3.3 LMH/bar R = 91.0 % S = 340 µm	PI Casting/overall thickness = 150/66.3 µm	2 M NaCl (10 mM NaCl)	500 mL/min	40.0	29.1	2013 [51]
Carboxylated CNTs (OD: 10-20 nm, L: 1-5 µm)	PES (MPD, TMC)	2 wt% in dope solution	A = 2.3 LMH/bar B = 0.08 LMH S= 2042 µm	PI Overall thickness = 90.1 µm	2 M glucose (10 mM NaCl)	2.0 cm/s	12.0	-	2013 [170]
Acid functionalized CNTs (D: ~11 nm, L: ~10 µm)	PEI (MPD, TMC)	0.3 wt% (weight ratio to PEI) in dope solution	A = 2.5 LMH/bar B = 0.7 LMH S = 310 µm	Electrospinning Flow rate = 30 µL/min Voltage = 30 kV Working distance = 12 cm Humidity = 60%	1 M NaCl (DI water)	9.0 cm/s	33.0	3.7	2015 [171]
Acid functionalized CNT/TiO_2 composites (OD: 9.5 nm, L: 1.5 µm)	PSf (MPD, TMC)	0.5 wt% in dope solution	-	PI Spin-coating at 3000 rpm for 1 s	1 M NaCl (DI water)	0.09 cm/s	12.7	5.8	2016 [172]
CNTs (D: 20 nm, L: 0.5-2 µm)	PSf (2 mg/mL DA Tris buffer solution, MPD, TMC)	0.15 wt% in dope solution	A = 6.5 LMH/bar B = 7 LMH S = 1669 µm	PI Casting thickness = 80 µm	2 M $MgCl_2$ (DI water)	7.8 cm/s	14.5	6.6	2016 [83]
HNT (ID: 5-15 nm)	PVDF (MPD, TMC)	0.5 wt% in dope solution	A = 2.02 LMH/bar B = 0.33 LMH S = 370 µm	PI Casting/overall thickness = 150/70-90 µm	2 M NaCl (10 mM NaCl)	350 mL/min	27.7	14.6	2016 [136]
Acid functionalized CNTs (n/a)	PES (MPD, TMC)	0.5 wt% in dope solution	A = 1.8 LMH/bar B = 1.89 LMH S = 387 µm	PI Casting thickness = 100 µm	0.6 M NaCl (DI water)	FS: 200 mL/min DS: 400 mL/min	11.98	7.7	2017 [173]

INTs (OD: 2 nm, ID: 1 nm, L: 100 -200 nm)	PSf (MPD, TMC)	0.66 wt% (weight ratio to PSf) in dope solution	A = 3.0 LMH/bar B = 2.9 LMH S = 2090 µm	PI Casting/overall thickness = 100/64.2 µm	1 M NaCl (DI water)	333.3 mL/min	7.5	11.6	2017 [174]
MOF: UiO-66 (507 nm)	PSf (MPD, TMC)	6.5 wt% (weight ratio to PSf) in dope solution	A = 3.31 LMH/bar B = 0.53 LMH S = 351 µm	PI Casting/overall thickness = 150/61 µm	1 M NaCl (DI water)	1.1 cm/s	24.5	4.4	2017 [175]
SiO_2/MWCNTs nano-rod (n/a)	PVDF (MPD, TMC)	0.75 wt% in dope solution	A = 1.21 LMH/bar B = 0.12 LMH S = 240 µm	PI Casting thickness = 150 µm	1 M NaCl (DI water)	300 mL/min	22.1	4.1	2018 [176]
Zwitterion (PMAPS) (n/a)	PES (MPD, TMC)	1.0 wt% in MPD solution	A = 0.69 LMH/bar B = 0.56 LMH	PI Casting/overall thickness = n/a	2 M NaCl (1,000 ppm oily WW)	32.7 cm/s	15.8 (AL-DS)	4.2 (AL-DS)	2018 [177]

A: water permeability coefficient; B: solute permeability coefficient; CFV: cross-flow velocity; CNT: carbon nanotube; DS: draw solution; FS: feed solution; HNT: halloysite nanotube; INT: imogolite nanotube; Js: solute flux; Jw: water flux; MF: microfiltration; MPD: m-phenylenediamine; MWCNT: multi-walled carbon nanotube; pDA: polydopamine; PEI: polyethylenimine; PES: polyether sulfone; PI: phase inversion; PSf: polysulfone; PVDF: polyvinylidene fluoride; S: structural parameter; TMC: trimesoyl chloride; TNT: titanate nanotube; WW: wastewater

Table 5: Summary of the fabrication conditions and FO performance of PA TFC membranes with non-porous nanomaterial-incorporated substrates.

TFC membrane with nanocomposite substrate		**Optimal particle loading**	**Intrinsic properties**	**Substrate fabrication method & conditions**	**FO performance (AL-FS)**				**Year [Ref]**
Filler embedded in substrate (Particle size)	**Substrate (PA layer monomers)**				**DS (FS)**	**CFV**	**Jw (LMH)**	**Js (gMH)**	
TiO_2 (~21 nm)	PSf (MPD, TMC)	0.5 wt% in dope solution	A = 1.98 LMH/bar B = 0.39 LMH S = 420 µm	PI Casting/overall thickness = 150/76 µm	2 M NaCl (10 mM NaCl)	32.72 cm/s	29.7	7.39	2013 [178] 2014 [179]
TiO_2 (~21 nm)	PSf (MPD, TMC)	0.6 wt% in dope solution	A = 2.63 LMH/bar B = 0.45 LMH S = 390 µm	PI Casting/overall thickness = 140/60-70 µm	2 M NaCl (DI water)	350 mL/min	33.0	15.7	2014 [180]
SiO_2 (160-240 nm)	Bottom layer: 10 wt% PSf	3 wt% in bottom layer and 0 wt% in top layer dope solution	A = 1.64 LMH/bar B = 0.29 LMH S = 169 µm	PI	1 M NaCl (DI water)	25 cm/s	31.0	7.4	2015 [181]

	Top layer: 7 wt% PSf (MPD, TMC)			Casting thickness of bottom/top layer = 0/80 µm on top of PET mesh Overall thickness = 97.2 µm					
GO (T: 1-2 nm)	PSf (MPD, TMC)	0.25 wt% (weight ratio to PSf) in dope solution	A = 1.76 LMH/bar B = 0.19 LMH S = 191 µm	PI Casting/overall thickness = 150/50 µm	1 M NaCl (DI water)	25.0 cm/s	29.5	5.5	2015 [52]
CN/rGO (n/a)	PES (MPD, TMC)	0.5 wt% (weight ratio to PES) in dope solution	A = 1.6 LMH/bar B = 0.3 LMH S = 163 µm	PI Casting/overall thickness = 100/51 µm	2 M NaCl (DI water)	-	41.1	9.6	2015 [182]
Zn_2GeO_4 nanowires (D: 20-50 nm, L: 200-300 nm)	PES (MPD, TMC)	0.05 wt% in dope solution	A = 2.47 LMH/bar B = 8.4 LMH S = 540 µm	PI Casting/overall thickness = 150/64 µm	2 M NaCl (DI water)	500 mL/min	21.6	4.0	2015 [183]
LDH/GO (T: 100-150 nm)	PSf (MPD, TMC)	2 wt% in dope solution	A = 0.53 LMH/bar B = 0.15 LMH S = 138 µm	PI Casting/overall thickness = 150/58.6 µm	1 M NaCl (DI water)	2.6 cm/s	13.4	6.2	2016 [184]
SiO_2 (200 nm)	PAN (MPD, TMC)	15 wt% (weight ratio to PAN) in dope solution	A = 2.5 LMH/bar B = 1.7 LMH S = 65 µm	Electrospinning Flow rate = 1 mL/h Voltage = 28.5 kV Working distance = 16 cm Humidity = 50%	1 M NaCl (DI water)	15.8 cm/s	56.2	8.2	2016 [185]
SiO_2 (n/a)	PAN (MPD, TMC)	15 wt% (weight ratio to PAN) in dope solution	A = 1.36 LMH/bar B = 0.88 LMH S = 29.7 µm	Electrospinning Flow rate = n/a Voltage = 20 kV Working distance = 15 cm Humidity = 47%	1 M NaCl (DI water)	7.5 mL/min	52	34.84	2016 [186]
GO (n/a)	PSf (MPD, TMC)	0.1 wt% in dope solution	-	PI Spin-coating at 3000 rpm for 1 s	0.6 M NaCl (DI water)	0.09 cm/s	3.6	1.7	2016 [172]
LDH nanoparticles (20-30 nm)	PSf (MPD, TMC)	2 wt% in dope solution	A = 0.61 LMH/bar B = 0.27 LMH S = 148 µm	PI Casting/overall thickness = 150/57.4 µm	1 M NaCl (DI water)	2.6 cm/s	18.1	8.1	2016 [187]
$CaCO_3$ (40– 80 nm)	PSf (MPD, TMC)	7.5 wt% in dope solution	A = 1.86 LMH/bar B = 0.77 LMH S = 796 µm	PI Casting thickness = 150 µm	2 M NaCl (DI water)	166.67 mL/min	17.0	44.3	2016 [188]

GO (T: 1-2 nm)	Bottom layer: 7 wt% PSf Top layer: 15 wt% PSf (MPD, TMC)	0.25 wt% in both top layer and bottom layers	A = 1.46 LMH/bar B = 0.25 LMH S = 130 µm	PI Casting thickness of bottom/top layer = 100/150 µm Overall thickness = 61 µm	1 M NaCl (DI water)	16.7 cm/s	33.8	6.9	2017 [189]
GO (n/a)	PSf (MPD, TMC)	0.5 wt% in dope solution	A = 0.54 LMH/bar B = 0.07 LMH S = 420 µm	PI Overall thickness = 70-90 µm	2 M NaCl (DI water)	2.5 cm/s	11.7	3.5	2017 [190]
TiO_2/GO (< 21 nm)	PSf (MPD, TMC)	0.5 wt% in dope solution	A = 0.58 LMH/bar B = 0.05 m/s S = 0.2 µm	PI Overall thickness = 70-90 µm	2 M NaCl (DI water)	2.5 cm/s	23.9	2.7	2017 [190]
Fe_3O_4 (20-30 nm)	PES (MPD, TMC)	0.2 wt% in dope solution	A = 3.06 LMH/bar B = 0.56 m/s S = 420 µm	PI Casting thickness = 100 µm on top of PE mesh Overall thickness = 99.47 µm	2 M NaCl (10 mM NaCl)	800 mL/min	28.8	14.7	2017 [191]
ZnO-SiO_2 core-shell (30 nm)	PES (MPD, TMC)	1.0 wt% (weight ratio to PES) in dope solution	A = 3.5 LMH/bar B = 4.0 LMH S = 297 µm	PI Casting/overall thickness = 100/59.8 µm	1 M NaCl (DI water)	8.3 cm/s	33.5	11.5	2017 [192]
SiO_2 (5-15 nm)	PEI (MPD, TMC)	1.6 wt% in dope solution	A = 2.99 LMH/bar B = 0.4 LMH S = 174 µm	Electrospinning Flow rate = 15 µL/min Voltage = 30 kV Working distance = 12 cm Humidity = 50% l = 93.7 µm D = 249 nm d_a = 1.28 µm	1 M NaCl (DI water)	9.0 cm/s	42.0	5.1	2017 [193]
TiO_2 (<25 nm)	PSf (MPD, TMC)	0.25 wt% in dope solution	n/a	Electrospinning Flow rate = 16.66 µL/min Voltage = 35 kV Working distance = 15 cm Humidity = 25%	1 M NaCl (DI water)	10.0 cm/s	51.5	12	2017 [63]
ZnO (50 nm)	PES (MPD, TMC)	1.0 wt% (weight ratio to PES) in dope solution	A = 3.1 LMH/bar B = 3.7 LMH	PI	1 M NaCl (DI water)	8.3 cm/s	31.2	12.6	2017 [192]

			S = 300 µm	Overall thickness = 70-90 µm					
TiO_2 (< 21 nm)	PSf (MPD, TMC)	0.5 wt% in dope solution	A = 1.5×10^{-12} m/s Pa B = 0.03 LMH S = 310 µm	PI Overall thickness = 70-90 µm	2 M NaCl (DI water)	2.5 cm/s	18.9	1.7	2017 [190]

815

816 A: water permeability coefficient; B: solute permeability coefficient; $CaCO_3$: calcium carbonate; CFV: cross-flow velocity; DS: draw solution; Fe_3O_4: iron (III) oxide, FS:
817 feed solution; GO: graphene oxide; Js: solute flux; Jw: water flux; LDH: layered double hydroxide; MPD: m-phenylenediamine; pDA: polydopamine; PAN:
818 polyacrylonitrile; PEI: polyethylenimine; PES: polyether sulfone; PI: phase inversion; PSf: polysulfone; rGO: reduced graphene oxide; S: structural parameter; SiO_2: silica;
819 TiO_2: titanium oxide; TMC: trimesoyl chloride; Zn_2GeO_4: zinc germinate; ZnO: zinc oxide

820

4.1 Zeolites, silica and zinc oxide

Several works have been published on zeolite-incorporated TFC membrane for RO applications because the unique pore structure of super-hydrophilic zeolite molecular sieves allows greater shape and size selectivity [194-197]. However, only two studies reported zeolite-modified PA TFC FO membrane, both of which were studied by Tang's group [45, 51]. Ma et al. were the first to prepare a nanocomposite substrate for TFC membrane to control ICP in the FO process [51]. The PA TFC membrane with an optimal porous zeolite loading of 0.5 wt% in the PSf substrate (PSfN0.5-TFC) demonstrated a water flux that was more than 2 times higher than that of the conventional TFC membrane. The structural parameter of the PSfN0.5-TFC (control TFC) membrane was found to be 340 μm (960 μm). The zeolite-loaded TFC membranes showed improvement in hydrophilicity, surface porosity and water permeability. However, the nanocomposite membrane was not highly selective, with a NaCl rejection of only ~91% attained using PSfN0.5-TFC membrane at 5 bar using a 10 mM NaCl feedwater [51].

Silica-modified PSf flat-sheet substrates have also been developed for PA TFC FO membranes. A dual-layered flat sheet membrane was made via the phase-inversion technique using silica-incorporated PSf solution for the bottom layer and pristine PSf solution for top layer [181]. The dual-layered TFC membranes had a much higher NaCl rejection (~98%) than the single-layered TFC membranes (~15-97%) at all silica loadings (1-4 wt%). However, only minor enhancement in water flux was attained in comparison to control membrane in AL-FS orientation for both single and dual-layered silica-modified TFC membranes. In contrast, water flux improved significantly in AL-DS orientation for nanocomposite TFC membranes compared to the pristine TFC membrane. The selectivity of single-layered silica-modified TFC membranes deteriorated with increasing silica concentration but remained nearly constant with dual-layered silica-incorporated membranes [198]. The better selectivity of the dual-layered substrate could be attributed to its desirable surface morphology for the formation of a high

salt rejecting and dense PA layer. Additionally, the porous and hydrophilic structure of the dual-layered substrate helped to reduce ICP.

More recently, electrospun silica-embedded nanofiber mats were prepared as porous substrates for PA TFC membranes [185, 193]. The low tortuosity and high porosity of the nanofiber mats substantially reduced ICP by reducing the structural parameter of the nanofiber supported membranes (<175 μm with the optimal silica loading). The high porosity of silica-nanofibrous substrate enhanced mass transfer within the support layer, which increased the osmotic water flux of FO membranes. The water and salt permeability of the best performing FO membrane increased by more than 7 and 3.5 times, respectively, in comparison to the commercial HTI-CTA FO membrane. The surface roughness of the silica-embedded nanofibers has not been reported in both the works; however, the high surface roughness is more likely to impair PA layer formation on the nanofibers support [199].

Rastgar et al. dispersed ZnO and ZnO-SiO_2 core-shell nanoparticles (ZSCSNPs) in the polyethersulfone (PES) substrate to explore the effect of different nanoparticle surface characteristics on the pore structure and performance of PA TFC FO membranes [192]. The cross-sectional SEM images exhibited dense sponge-like porous structure for pristine PES substrates and loose and long finger-like porous structures for ZnO and ZSCSNPs-incorporated substrates. The hydrophilicity and large surface area of ZnO and ZSCSNPs could have augmented the exchange rate of solvent/non-solvent phases during the phase-inversion process that resulted in the development of finger-like pore structures. The finger-like pore structures reduced ICP by decreasing membrane tortuosity and structural parameter. The water fluxes of ZnO and ZSCSNPs-incorporated TFC membranes were more than twofold higher than that of the pristine TFC membrane. The TFC membrane with 1.0 wt% ZNCSNPs loading had higher hydrophilicity, permeability, pore density, and bigger surface pore size compared to the 1.0 wt% ZnO loaded TFC membrane. Although the ZnO nanoparticles had 10 times higher surface

871 area than the ZNCSNPs, the water fluxes obtained using ZNCSNPs-modified TFC membranes
872 were higher with comparable solute flux. Hence, the impact of nanoparticle hydrophilicity on
873 the FO performance was found to dominate the effect of surface area.

874 *4.2 Carbon nanotubes and graphene oxide*

875 Unlike conventional PA TFC membranes supported on polymeric substrates (PSf/ PES),
876 novel membranes with PA layer supported on robust and highly stable self-supporting Bucky-
877 papers (BPs) were fabricated for potential application in FO/RO processes by Dumée et al.
878 [55]. The BPs were solely comprised of hydroxyl-functionalized entangled CNTs that
879 demonstrated enhanced wettability (contact angle < 20°) after plasma treatment. The high
880 porosity of BPs allowed good water permeation (water uptake capacity of 17%), and the
881 comparable pore size of BPs and PSf support meant that the PA layer could effectively form
882 on BP without damage. The BP supported PA TFC membranes also had a smoother surface
883 (29.2 nm) than the PSf-supported (56 nm) and commercial TFC membranes (49.7 nm). The
884 low structural parameter (620 μm) for BPs could potentially reduce ICP. Additionally, the
885 water and salt permeability of BPs could be adjusted by preparing thin sheets and fine-tuning
886 their chemistry. Nonetheless, no data on water flux and salt rejection have been provided for
887 FO performance tests possibly due to the membrane's fragility.

888 It is essential to functionalize CNTs to improve their hydrophilicity before blending them
889 in the polymer dope solution in order to improve the performance of CNT-incorporated FO
890 membranes. Pristine CNTs are hydrophobic and form low porosity substrates with macrovoids
891 that increase draw solute leakage and reduce water flux. Moreover, pristine CNTs can readily
892 agglomerate in organic and/or polymer solutions [172]. Wang et al. produced a high-
893 performance PA TFC membrane for desalination using carboxylated MWCNTs-blended PES
894 substrates [200]. The nanomaterial-incorporated substrates were observed to have finger-like

macrovoid structures that resulted in better water permeability, higher salt rejection (>90%), and smaller structural parameter than the neat PES and CTA commercial membrane. The open porous structure of the substrate significantly reduced ICP and improved water flux. The nanomaterial-incorporated PES substrate also demonstrated higher tensile strength; thus, creating the possibility of producing substrates without fabric supports.

Similarly, Choi et al. used carboxylated MWCNTs (f-MWCNTs) incorporated PA TFC membrane for application in combined seawater desalination and wastewater recovery FO process [173]. The increased porosity and hydrophilicity of the nanocomposite membrane resulted in a 72% higher water flux than the baseline TFC membrane. The SRSF of nanocomposite membrane was 15% lower than the TFC membrane. The nanocomposite membrane also exhibited 19% less decline in normalized flux under alginate fouling test compared to TFC membrane because of the negatively-charged membrane surface, which improved repulsive foulant–membrane interaction. The smoother surface and electrostatic repulsive force of the nanocomposite membrane improved fouling reversibility, and the recovered normalized flux of nanomaterial-incorporated TFC membrane was observed to be 6% higher than TFC membrane after physical cleaning.

Polyetherimide (PEI) nanofibers embedded with f-MWCNTs were also explored as potential substrates for PA TFC membranes [171]. The f-MWCNTs were found to be well-distributed in the nanofibers, which improved the average substrate porosity and tensile strength by 18% and 53% respectively and decreased the structural parameter by 30% compared to neat PEI nanofibers. The dispersed f-MWCNTs retained the porous structure by providing better compaction resistance to nanofibers during heat-press treatment. The nano-sized water channels of f-MWCNTs could have also contributed to the higher substrate porosity and improved pure water permeability. The high mechanical strength of f-MWCNTs-incorporated nanofibers assisted in ICP mitigation by allowing a further increase in substrate

porosity and pore size and forming large interconnected pores. As a result, the water flux of nanomaterial-incorporated TFC membranes was much higher than neat TFC membranes. The nanomaterial-incorporated TFC membranes also demonstrated a lower SRSF than the control TFC membrane.

In addition to CNTs, graphene derivatives like graphene oxide (GO) and reduced GO (rGO) have been explored as potential nanofillers for TFC FO membrane substrate due to their smooth structure, high mechanical strength, good chemical stability, low thickness (1-2 nm), favourable surface chemistry and high surface area-to-volume ratios that assist in better interaction with the polymer matrix [201-204]. GO's surface contains hydrophilic oxygen-containing functional groups like epoxide, carbonyl, hydroxyl and carboxyl groups, which can improve the hydrophilicity and antifouling properties of the nanocomposite membranes [205].

Recent studies have reported that GO incorporation into TFC substrate enhanced the membrane pore diameter, porosity, and hydrophilicity, which markedly increased water permeability and allowed efficient formation of PA layer [52, 172, 190]. Moreover, the addition of GO/TiO_2 composite and/or mixture to membrane substrate further improved the water flux, compared to pristine and GO-modified TFC membrane, without significantly sacrificing the reverse solute flux due to the establishment of straight finger-like elongated pores and increased the support layer porosity [172, 190]. A similar observation was made using rGO modified graphitic carbon nitride (CN/rGO) as PES substrate filler, which reduced membrane structural parameter by changing the PES substrate structure [182].

Lim et al. developed a TFC FO membrane with a dual-layered nanocomposite substrate [189] as shown in Figure 8. The substrate layers were made using 15 wt% and 7 wt% PSf solution for the top and bottom layers, respectively. The lower PSf concentration of the bottom layer resulted in the creation of highly porous finger-like structures, which helped diminish

944 ICP effects. Whereas, the higher concentration of PSf in the top layer formed a smooth, thin
945 skin layer with desirable pore size for adequate development of the dense PA layer. The pure
946 water permeability and porosity of the dual-layered membrane substrate were suggestively
947 higher than the single-layered substrate. Dual-layered TFC membrane incorporated with 0.25
948 wt% hydrophilic GO nanosheets demonstrated a lower structural parameter, higher water
949 permeability and ion selectivity compared to the GO-free membrane. The water flux of GO-
950 modified dual-layered TFC membrane was 69% higher than the single-layered TFC membrane
951 under AL-FS mode using 1 M NaCl and DI water as a draw and feed solution, respectively.
952 Moreover, the reverse solute flux of GO-modified dual-layered TFC membrane was less than
953 that of single-layered TFC membrane under the same operating conditions suggesting that
954 improvement in water permeability was achieved without comprising on membrane selectivity.
955 The dual-layered PSf substrates were also able to mitigate the ICP effects at higher draw
956 solution concentrations effectively.

957

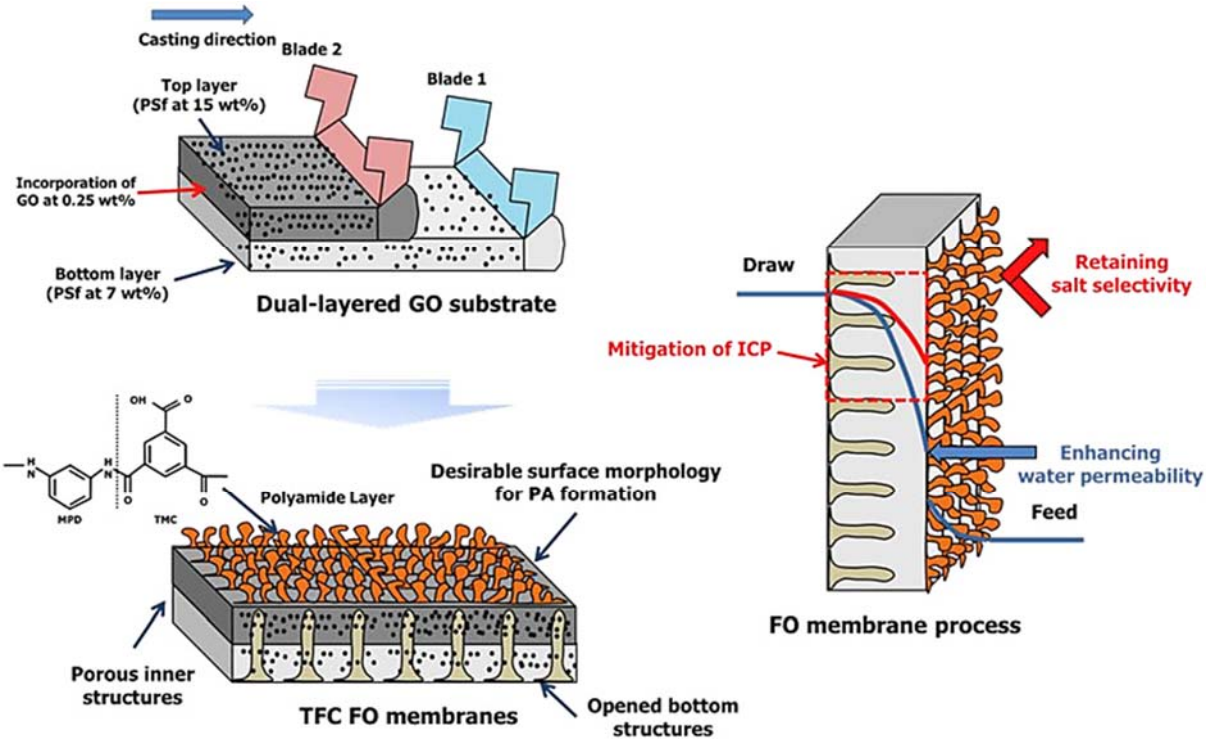

Figure 8: Schematic of the co-casting technique used for fabrication of dual-layered GO-incorporated TFC FO membranes [189].

4.3 Titanium oxide

TiO_2 nanoparticles have been extensively used to enhance characteristics of RO, NF, UF, membrane distillation (MD), pervaporation, and FO membranes due to their outstanding hydrophilicity, good anti-fouling properties, high chemical stability and adequate photochemical reactivity [206-210]. Ismail's group was the first to incorporate TiO_2 nanoparticles in the PSf substrate of PA TFC membrane using direct blending to control ICP in the substrate during FO operation [178, 180]. Similar to MWCNTs and GO, incorporation of TiO_2 in the membrane substrate formed long finger-like pores, improved hydrophilicity and porosity [180]. The structural parameter of 0.5 wt% TiO_2 embedded membrane was found to be 420 µm, which was much smaller than that of the TFC membrane (980 µm). The water flux of nanocomposite membrane embedded with 0.5 wt% TiO_2 was approximately 87% higher

than the TFC membrane in AL-FS mode when tested using 10 mM and 0.5 M NaCl as feed and draw solution, respectively. In addition, the TFN membrane demonstrated good water flux stability under long-term FO test due to diminished effect of ICP in the support layer [178]. Increasing the TiO_2 loading beyond 0.5 wt% caused in particle agglomeration at the surface of the substrate causing a lower degree of cross-linking in the PA layer. Consequently, water flux increased but at the expense of deteriorating membrane selectivity [211].

Additionally, the TiO_2-embedded TFC membrane was tested for organic fouling in AL-DS mode using BSA in the presence of Ca^{2+}. The hydrophilic nature of the nanocomposite membrane significantly diminished the hydrophobic BSA adsorption on the membrane surface. The fouling in nanocomposite membrane was highly reversible with a pure water flux recovery of 92% after rinsing with water for 30 minutes without any chemical cleaning reagents; while the control TFC membrane achieved a water flux recovery of 79% [179].

4.4 Other nanomaterials

A Zn_2GeO_4 nanowire embedded PSf UF membrane with high surface porosity was employed as a substrate for PA TFC FO membrane preparation. The surface characteristics of the substrate improved the crosslinking-degree of PA layer that improved membrane selectivity. However, the Zn_2GeO_4 nanowire-modified substrate demonstrated a lower FO water flux despite achieving a water permeability that was ~42% higher than that of the control PES membrane in RO mode. The contradicting results may have occurred as the Zn_2GeO_4 incorporated substrate failed to efficiently mitigate ICP due to the increased membrane tortuosity resulting from the formation of thick pore walls near the bottom matrix of the membrane. The modified membrane also had a higher structural parameter (540 vs. 352 μm) than the pristine PES membrane [183].

In another study, hydrophilic HNTs were embedded into a PSf substrate with an optimal loading of 0.5 wt%. Increasing the HNTs loading beyond 0.5 wt% resulted in poor salt rejection due to a lower degree of cross-linking in the PA layer. The structural parameter of 0.5 wt% HNT-incorporated membrane (370 μm) was lower than that of the control TFC membrane (950 μm) due to higher porosity, enhanced hydrophilicity and extra water pathway formation in the substrate. The HNT-modified membrane also exhibited high water permeability without significantly sacrificing membrane selectivity. The water flux of nanocomposite membrane was much higher than that of the control TFC membrane in both AL-FS (27.7 vs. 13.3 $Lm^{-1}h^{-1}$) and AL-DS (42.3 vs. 26.0 $Lm^{-1}h^{-1}$) orientations when 10 mM and 2 M NaCl were used as feed and draw solution, respectively [136].

Wang and co-workers developed functional layered double hydroxide (LDH) nanoparticles blended PSf UF substrates for TFC FO membranes [187]. Addition of LDH changed the substrate morphology, which significantly enhanced the surface pore diameter, surface hydrophilicity, porosity, thermal stability and mechanical strength of the membrane. The water permeability of nanocomposite membranes was higher than the pristine TFC membrane at all LDH loadings (0 – 4 wt%). The water flux of the optimal LDH-modified membrane (2 wt% LDH loading) was 42.5% more than that of pristine TFC membrane when tested in AL-FS orientation with DI water and 1 M NaCl as feed and draw solution, respectively. The structural parameter of the 2 wt% LDH loaded membrane, and the pristine membrane was evaluated as 148 μm and 287 μm, respectively. Integration of LDH in the membrane substrate reduced the substrate tortuosity and ICP effects [187]. The group also synthesized LDH/GO hybrid as a nanofiller for PSf substrate and obtained similar results as the LDH-modified substrate. However, the LDH/GO-modified membrane exhibited a lower structural parameter (138 μm) and reverse solute flux compared to the LDH-modified and pristine TFC membranes [184].

Imogolite nanotubes (INTs) are hydrous aluminosilicate single-walled nanotube materials that have evolved as a promising competitor of CNTs [212]. Unlike CNTs, INTs are exceptionally hydrophilic due to the existence of ample hydroxyl groups both on their outer and inner walls (Figure 9). In addition to their superior hydrophilicity, INTs have a high aspect ratio and surface area that make them potential nanofillers for developing desalination membranes [213, 214]. Pan et al. prepared hydrophilic TFC FO membranes for desalination using INTs blended PSf substrates [174]. It was found that the TFC membrane with 0.66 wt% INTs blended PSf substrate demonstrated the best FO performance regarding water flux and salt rejection. Moreover, the incorporation of INTs in the substrate enhanced the intrinsic transport properties of the nanocomposite membrane. The INTs blended substrates provided three types of passages for salt and water transport. The first type included the widest channels that are formed during the phase inversion process and comprised of the finger-like pores, top surface spongy pores, and bottom surface macro-voids. The second kind involved the interfacial gaps, which existed between the INTs and the polymer matrix; whereas, the third type comprised of the INTs nanochannels. The interfacial gaps and INTs nanochannels helped to connect the wide channels or pores in the substrate polymer matrix to assist in water and salt transport. Incorporation of INTs alleviated ICP as the optimal nanocomposite membrane had a much lower structural parameter (2.09 mm) than the TFC membrane (13.34 mm) [174].

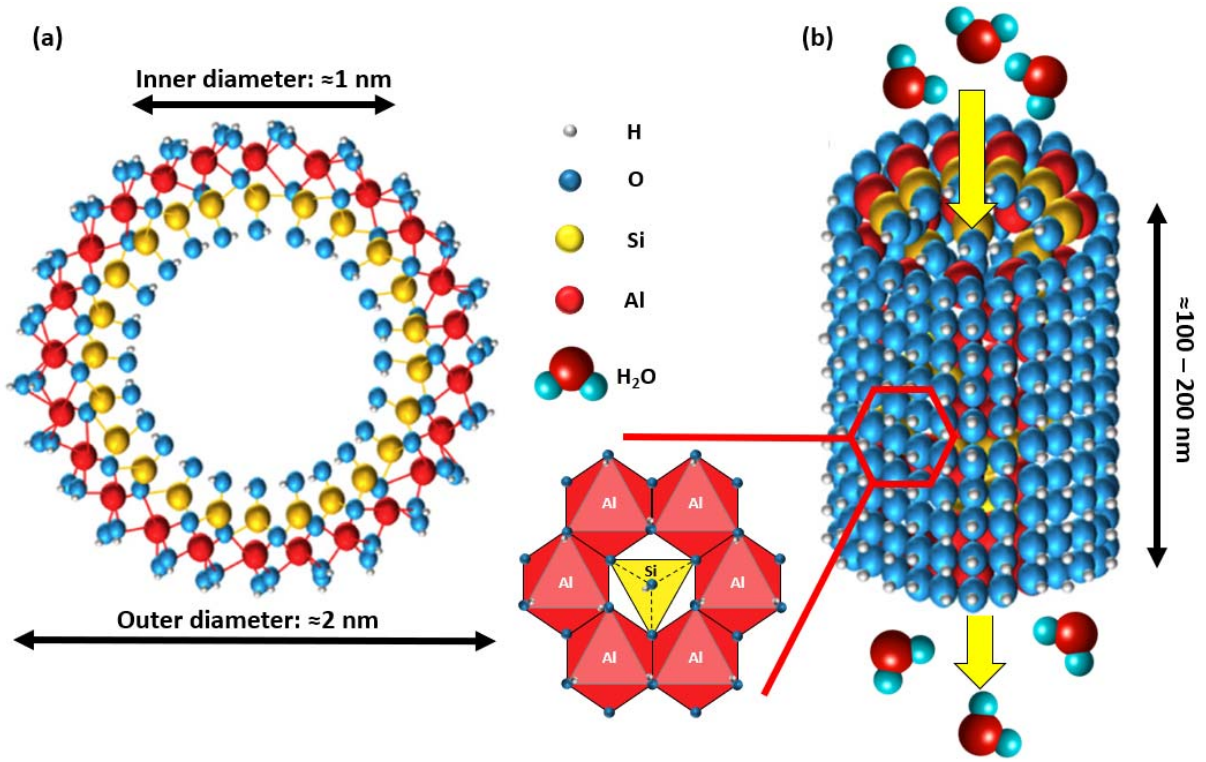

Figure 9: View of the atomic structure of INTs. (a) Axial and (b) 3-D side view (adapted from [174]).

The work of Deng et al. [215] on the development of ultrahigh permeable nanoporous membranes using copper hydroxide nanostrands as sacrificial additives inspired Kuang et al. to develop porous PSf substrates using calcium carbonate nanoparticles ($CaCO_3$-NPs) as sacrificial additives [188]. The $CaCO_3$-NPs distributed in PSf matrix were removed after the phase inversion process by etching with hydrochloric acid to enhance the substrate porosity. Chemical etching of the substrate reduced the membrane structural parameter. Increasing the $CaCO_3$-NPs loading made the substrate more porous and reduced the structural parameter further. The optimal membrane with a 7.5 wt% $CaCO_3$-NPs loading demonstrated a water flux of 17 $Lm^{-1}h^{-1}$ (27.6 $Lm^{-1}h^{-1}$) in AL-FS (AL-DS) mode compared to a much smaller water flux of 3.6 $Lm^{-1}h^{-1}$ (5.5 $Lm^{-1}h^{-1}$) obtained using the control TFC membrane under same testing conditions. Although the sacrificial additive helped to increase the membrane porosity and water flux, it hampered membrane selectivity. The salt permeability of the modified

membranes was much higher than the control membrane, and the SRSF values were reported between 3 g/L and 2.3 g/L at different $CaCO_3$-NPs loading in AL-FS mode, which is much higher than those reported in other FO nanocomposite membrane studies [188].

Ferrous-ferric oxide (Fe_3O_4) has also be used as a nanofiller in PA TFC membrane substrate due to its numerous desirable properties like high surface area, low toxicity, chemical stability, good biocompatibility and magnetic properties. Darabi et al. added Fe_3O_4 nanoparticles (0.06-0.5 wt%) in the PES substrate matrix to alleviate ICP. The water and salt permeability increased as the Fe_3O_4 loading was increased from 0-0.2 wt% due to higher overall porosity and formation of additional water pathways that considerably reduced the membrane structural parameters from 780 to 420 µm. The lowest NaCl rejection (93.2%) was observed at 0.2 wt% Fe_3O_4 loading due to particle agglomeration that reduced the degree of PA cross-linking. Increasing the Fe_3O_4 loading beyond 0.2 wt% increased the structural parameter from 420 to 850 µm, decreased water permeability and improved salt rejection possibly due to pore blockage and reduction in the overall membrane porosity. The nanocomposite membrane with 0.2 wt% Fe_3O_4 loading demonstrated the highest water flux and lowest SRSF compared to other membranes. [191].

4.5 Issues and challenges of nanomaterial-modified substrates

One of the major drawbacks of nanocomposite substrates is that a comparatively higher nanomaterial loading is required compared to the TFN membranes to observe any improvement in membrane performance. The relatively high cost of fabricating TFC membranes with nanocomposite substrates may limit their wide applications. In addition, nanoparticles may agglomerate easily in polymer dope solution due to the solution viscosity and the polymer-nanoparticle incompatibility. Therefore, interfacial voids are formed between the nanomaterial and the polymer, which can cause nanoparticle loss and reduce membrane selectivity. In addition, some nanomaterials can change substrate morphology and increase surface pore size, which will result in the formation of defective PA layer during the IP process. Hence, it is preferable to use organic pore formers like PVP and polyethylene glycol (PEG) to prepare a

substrate with a porous bottom surface and a tight top surface for the formation of a defect-free PA layer [216, 217]. Moreover, cost-effective nanoparticles can be developed that are hydrophilic and compatible with polymer-phase to reduce ICP and minimize material loss.

5. Nanomaterial interlayer

Although commercial TFC FO membranes have demonstrated exceptional separation performance, their practical application is still challenging due to their intrinsic trade-off effect between water flux and salt flux. Further improvement in water permeability without reducing selectivity is difficult by only embedding nanomaterials in the membrane active layer or substrate. Besides nanomaterial modification of TFC membranes, several studies have focused on the development of the PA layer structure performance enhancement of TFC membranes by optimizing the IP process conditions. It was found that parameters like the monomer concentration, reaction time and temperature considerably affect the PA layer formation because IP is a diffusion-controlled process where the amines in the aqueous phase diffuse to the organic phase and react with the acyl chloride at the interface between aqueous and organic solutions [36, 218, 219]. In addition, the surface property and pore structure of the substrate surface facing the active layer directly influences the PA layer structure because it serves as a platform for holding the aqueous amine solution during the IP reaction. For example, large pores on the substrate surface can cause the PA to develop inside the porous substrates and form a defective selective layer. Therefore, efforts have been made to fine-tune the surface properties of substrates using nanomaterial-based interlayer between the porous substrate and dense PA layer to form a defect-free PA active layer through controlled IP reaction. Figure 10 illustrates the typical steps involved in the fabrication process of PA TFC membranes incorporated with a nanomaterial interlayer.

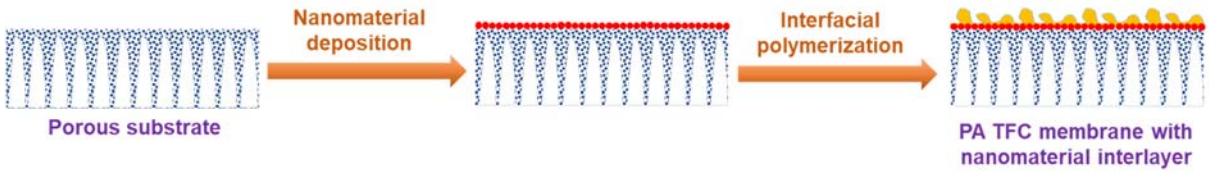

Figure 10: Typical steps involved in the preparation of a PA TFC membrane incorporated with a nanomaterial interlayer.

5.1 Carbon nanotubes and graphene oxide

Livingston's group recently developed a free-standing PA layer, less than 10 nm thick, via controlled IP reaction on top of a porous cadmium hydroxide nanostrand layer coated on a porous substrate [49]. The nanostrand interlayer allowed the development of an ultrathin, uniform and defect-free PA active layer through controlled release of MPD solution at the water-hexane interface, which exhibited excellent permeability. Inspired by this study, Zhao et al. developed a TFC membrane using a CNT interlayer between the polyvinylidene fluoride (PVDF) support layer and PA layer [220]. The CNT interlayer improved the effective contact area of the PA layer area by providing a porous three-dimensional free space below the PA skin. The structural parameter of the modified membrane (392 μm) was significantly lower than the control membrane (1562 μm) because the CNT interlayer free-space acted as a buffering zone to enhance the feed and draw solution exchange near the PA active layer and maintain the osmotic pressure; thus, diminishing the ICP effect in the FO process [220].

Meanwhile, Zhang and co-workers deposited GO/MWCNT composite as an intermediate layer on MF support using vacuum filtration to facilitate the successful growth of defect-free PA layer on substrates with large pores [221]. The GO/MWCNT layer controlled the diffusion of MPD by forming hydrogen and/or covalent bonds with the MPD monomers that contributed towards the formation of a thinner PA layer. Moreover, the GO/MWCNT layer prevented the diffusion of TMC inside the substrate pores that restricted the PA growth along the

GO/MWCNT layer but not within the substrate pores (Figure 11). Consequently, the FO membranes with the interlayer demonstrated higher water flux and better selectivity than the control membranes. The nanochannels in the MWCNT/GO interlayer also contributed towards enhanced water flux of the modified membranes.

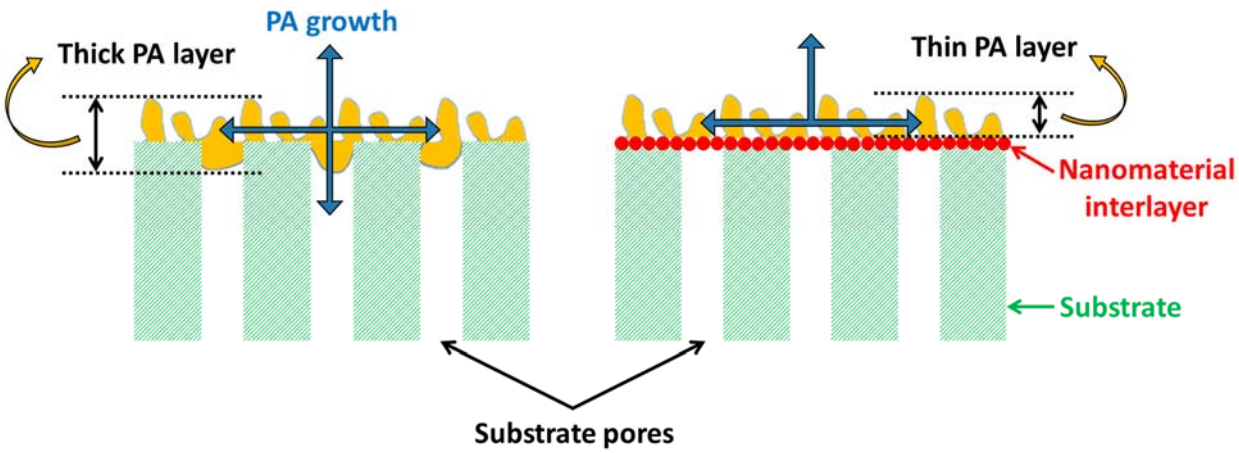

Figure 11: Schematic diagram representing the PA development process on porous substrates with and without a nanomaterial interlayer.

A similar mechanism was reported by Zhou et al. who spray-coated an ultrathin CNT interlayer onto a commercial porous PES MF membrane using an airbrush to develop a high-performance TFC FO membrane [222]. The CNT interlayer not only prevented the PA formation into the substrate pores but also enhanced the effective PA surface area, which reduced the water transport resistance. The crosslinking degree of the PA layer formed on the CNT interlayer was found to be higher than that on the PES substrate. The resulting TFC membrane with the CNT interlayer exhibited 7 times higher water flux and 7 times lower SRSF than that of the control TFC membrane in AL-DS mode with DI water and 1 M NaCl as feed and draw solution, respectively.

Subsequently, Choi et al. formed a hydrophilic pDA/GO interlayer on the PSf support [223]. They found that increasing the pDA coating time and GO loading beyond 1 h and 0.5

g/L, respectively, resulted in the reduction of water permeability due to blockage of surface pores by pDA and GO. The TFC membranes with pDA/GO interlayer demonstrated improved water flux without affecting the selectivity when GO loading was maintained between 0.25 g/L and 0.5 g/L with a pDA coating duration of 1 h.

5.2 Porous coordination polymers

More recently, Wang et al. suggested the construction of an interlayer on PSf substrate using MOF UiO-66 nanoparticles for preparing TFC FO membranes [224]. The optimal TFC membrane with UiO-66 interlayer showed better water flux, selectivity and lower transport resistance than both the pristine and UiO-66 modified TFN membranes. The channels of UiO-66 nanoparticles allow water molecules to pass through while rejecting the hydrated draw solute ions. Future studies can focus on tuning the properties and structure of the PA layer by modifying the properties of the interlayer, such as its surface pore size, roughness and thickness, to achieve high membrane performance.

5.3 Issues and challenges of nanomaterial interlayer

The scalability of nanomaterial interlayer development on porous substrates may be very challenging. Vacuum filtration is the most widely used technique used to deposit nanomaterial interlayer, but its implementation for large-scale membrane production may be unviable. A more feasible strategy may be to use controlled spray coating, which can be easily installed in the commercial membrane fabrication unit. Besides scalability, the material should be carefully selected for interlayer formation such that they provide a desirable platform of defect-free PA layer formation without causing pore blockage.

6. Implications and future perspectives

Figure 12 summarises the critical issues in the fabrication of nanomaterial-incorporated PA TFC membranes that need addressing to achieve further enhancement in the membrane

performance and scalability. Particle aggregation is one of the major issues encountered during nanocomposite membrane fabrication, and it mainly results from the high surface energy of nanomaterials and high inter-particle interactions. This results in poor dispersion of nanofillers in the monomer solution used for PA layer formation, or in the polymer dope solution used for membrane substrate. Agglomeration of nanoparticles decreases the effective nanoparticle surface area and results in the formation of a defective PA layer with voids and uneven nanomaterial distribution. Several studies have explored surface functionalization of nanomaterials like amine-functionalized or carboxylated CNTs and HNTs to minimize particle aggregation in the non-polar solvent or polymer matrix and produce dense defect-free active layer. Besides surface functionalization of nanofillers, new nanomaterials like MOFs and COFs can be designed with customized pore structure and surface charge to facilitate homogenous distribution of nanofillers in the polymer matrices. In addition, more surface modification methods can be explored to overcome the trade-off relationship between water and solute flux, and improve the anti-fouling property and chlorine resistance of the PA TFC membranes.

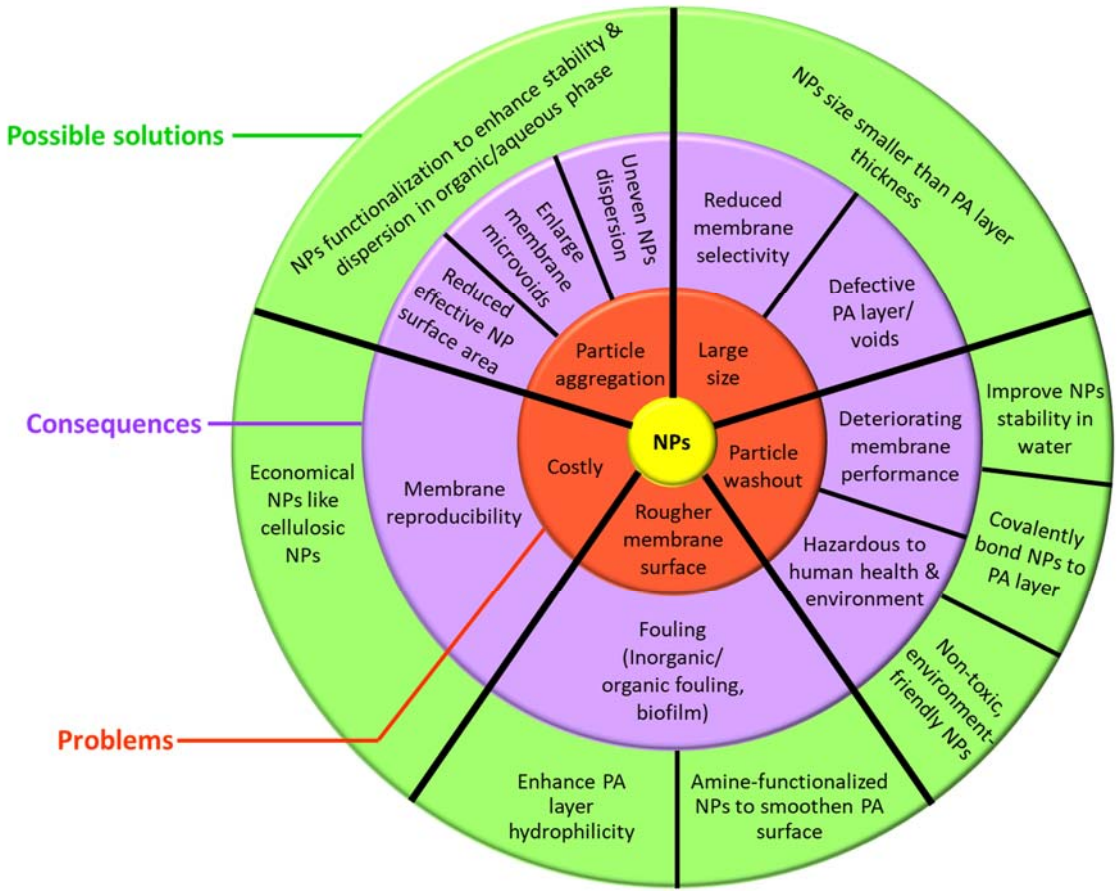

Figure 12: Current problems and consequences of nanoparticle (NP) incorporation in the membranes, and some possible solutions to overcome those issues.

Non-uniform nanomaterial dispersion in the solvent or polymer dope solution can hinder membrane reproducibility and cause a significant amount of variation in the FO performance, especially when a small FO membrane coupon is used for performance tests. For instance, if coupons are tested from a membrane sample with a non-uniform nanoparticle dispersion, then coupons cut from the membrane region with a denser nanoparticle loading will demonstrate higher water flux comparatively. Hence, it is crucial that all lab-scale membrane performance studies are conducted using larger membrane samples instead of small membrane coupons like

2 cm^2 so that the performance results are comparable and representative of the whole composite membrane.

The size of nanoparticle not only affects the substrate morphology but also influences the development of PA active layer. Consequently, it is vital to ensure that particles smaller than the PA layer thickness (150-300 nm) are used so that they can be effectively incorporated into the PA layer. Nanofillers larger than the PA layer thickness, such as CNTs and HNTs can damage the active layer and undermine membrane selectivity [225, 226]. The loss of nanomaterials during membrane fabrication and FO operation is an additional problem. For example, a large amount of hydrophilic nanomaterial dispersed in the aqueous amine solution for the IP reaction can be lost from the substrate surface when the surplus amine solution is removed using a rubber roller. As a result, only a small quantity of the nanomaterials would remain inside the substrate pores.

Many works that have used hydrophilic nanotubes (functionalized CNTs and HNTs) as membrane fillers have stated that incorporation of nanotubes into the membrane substrate or PA layer can improve water permeability without significantly affecting salt rejection by providing extra passages for transport of water molecules [81, 227]. However, the concept of the preferential pathway for water molecules requires further verification since it is only possible if the nanochannels are aligned towards the water flux direction and not blocked by the polymer matrix they are embedded in. So far, most studies on liquid separation reported the membrane performance results with only randomly arranged nanotubes [79, 83, 220]. Sharma et al. used an electric field to align CNTs in the polymer membranes for hydrogen separation [228]. Thus, it may be possible to use an electric or magnetic field to consider the effect of uniform nanotube alignment on the membrane performance for liquid separation.

Although FO process is associated with an intrinsic low fouling potential, FO process performance can be significantly affected by the reduced mass transfer resulting from the fouling layer resistance and increased concentration polarization [68, 229]. The addition of hydrophilic nanomaterials in the PA selective layer can significantly improve the membrane hydrophilicity but may also increase the surface roughness, which can promote fouling and exacerbate biofilm formation [35].

While many studies have developed and tested nanocomposite PA TFC membranes at a lab-scale level, nanomaterial-incorporated TFC membranes are not yet reported on a commercial scale, which raises concerns on the economic competitiveness of the nanocomposite membranes. Although reproducibility and cost-effectiveness of the nanocomposite membrane are important, it is also crucial that the long-term performance of the nanocomposite membranes under real feed conditions are well understood to determine membrane robustness. Long-term performance tests and thorough assessment of the nanocomposite membrane stability are critical, especially for the surface-modified nanocomposite membranes, to control leaching of nanomaterials. Leaching of nanomaterial may deteriorate membrane performance and durability. For example, depletion of biocidal agents like AgNPs located on the membrane surface can result in loss of membrane antimicrobial activity with time. Thus, it is worth exploring and developing surface coating materials that firmly adhere to membrane surface that are stable in water, can resist fouling and chlorine attack.

Additionally, it is essential to develop reliable and standard protocols for characterizing FO membranes to facilitate the standardization of the results obtained from different research groups and enable data exchange and analysis. Kim et al. comprehensively reviewed the various approaches available to determine the characteristics of FO membranes [230]. The RO-FO tests are the most widely used methods to estimate the intrinsic membrane transport and

structural parameters. However, the intrinsic parameters obtained for FO membranes using the RO-FO tests are unreliable due to the different driving forces used in the RO and FO process. Moreover, testing the FO membranes at high hydraulic pressures can damage the thin active and support layer of the membrane, which will result in unreliable estimation of membrane transport and structural parameters [231]. To address these issues, Tiraferri et al. proposed a non-pressurized method comprising of a four-step FO protocol, where a different draw solution concentration is used in each step [232]. Non-linear least-squares regression is then performed using the experimental water and reverse salt flux data obtained in each step to estimate the intrinsic membrane transport and structural parameters. Nonetheless, the four-step FO protocol is unsuitable for predicting the performance parameters of pressure-applied FO processes. Kim et al. have extensively discussed in their review the limitations of the existing protocols and other possible methods to determine FO membrane characteristics [230]. Furthermore, a standard protocol for FO operating conditions is also required to be able to compare different membranes in terms of FO performance. For instance, a predetermined cross-flow velocity should be used for all studies as it has a significant impact on the mass transfer and mixing of feed and draw solution in the flow channels, which will ultimately affect the water flux, solute flux and membrane fouling.

7. Conclusions

In this paper, we reviewed the development of nanomaterial-incorporated PA TFC membranes for FO processes. We focused on different nanofillers and the methods used to fabricate nanocomposite membranes. In addition, we discussed the influence of various nanoparticles on the performance and anti-fouling property of the membranes. Most studies observed that incorporation of nanofillers into the TFC membranes changed membrane physicochemical properties resulting in a more durable and high-performing TFC membrane with good anti-fouling property. Several studies also reported that the nanomaterial-

incorporated PA TFC membranes can overcome the trade-off between membrane permeability and selectivity that occurs in the conventional TFC membranes; although, their fundamental mechanisms are yet to be fully understood.

The fabrication of nanocomposite membrane, however, faces several challenges. Hence, the commercialization of nanocomposite membranes for industrial-scale application will not be possible unless those challenges are addressed. Some of the major challenges include the high nanomaterial cost, toxicity, and the additional nanomaterial modification steps required to fabricate nanocomposite membranes. Besides, the nanoparticle used should be highly dispersible in the solvent or polymer dope solution and have high polymer-nanoparticle compatibility to prevent the non-uniform distribution of nanomaterials within the membrane material. Most of the approaches adopted for lab scale fabrication of nanocomposite membrane may not be scalable; hence, such methods could need significant modifications.

The robustness and stability of surface modified nanocomposite membranes to the long-term operation is another significant concern that needs to be addressed through long-term studies. Most of the published works have not reported the robustness of the nanocomposite membranes, including their ability to meet the stringent health and safety for drinking water standards. The loss of nanomaterials during fabrication not only adds to the membrane cost but could be a significant health issue if leached during the FO operation.

Overall, this review shows that the nanocomposite membranes have the potential for much-improved membrane performance compared to the conventional TFC FO membranes. However, more research is required to improve our understanding of the nanoparticle-polymer interactions, its effect on water/solute transport mechanism and membrane fouling so that the membrane design and performance can be improved for specific applications.

Acknowledgments

The research reported in this paper was supported by the King Abdullah University of Science and Technology (KAUST), Saudi Arabia, through the Competitive Research Grant Program – CRG2017 (CRG6), Grant # URF/1/3404-01. H.K.S and Y.C. acknowledge the support provided by the Australian Research Council under the Future Fellowships scheme (FT140101208 & FT160100107), ARC Industry Hub (IH170100009) and Discovery Project (DPDP180102210).

References

[1] M.G. Buonomenna, J. Bae, Membrane processes and renewable energies, Renewable and Sustainable Energy Reviews, 43 (2015) 1343-1398.
[2] A. Subramani, J.G. Jacangelo, Emerging desalination technologies for water treatment: A critical review, Water Research, 75 (2015) 164-187.
[3] A. Ali, R.A. Tufa, F. Macedonio, E. Curcio, E. Drioli, Membrane technology in renewable-energy-driven desalination, Renewable and Sustainable Energy Reviews, 81, Part 1 (2018) 1-21.
[4] N.L. Le, S.P. Nunes, Materials and membrane technologies for water and energy sustainability, Sustainable Materials and Technologies, 7 (2016) 1-28.
[5] C.A. Quist-Jensen, F. Macedonio, E. Drioli, Membrane technology for water production in agriculture: Desalination and wastewater reuse, Desalination, 364 (2015) 17-32.
[6] D. Attarde, M. Jain, P.K. Singh, S.K. Gupta, Energy-efficient seawater desalination and wastewater treatment using osmotically driven membrane processes, Desalination, 413 (2017) 86-100.
[7] K.P. Lee, T.C. Arnot, D. Mattia, A review of reverse osmosis membrane materials for desalination—Development to date and future potential, Journal of Membrane Science, 370 (2011) 1-22.
[8] S. Liyanaarachchi, L. Shu, S. Muthukumaran, V. Jegatheesan, K. Baskaran, Problems in seawater industrial desalination processes and potential sustainable solutions: A review, Reviews in Environmental Science and Bio/Technology, 13 (2014) 203-214.
[9] M.M. Motsa, B.B. Mamba, A. D'Haese, E.M.V. Hoek, A.R.D. Verliefde, Organic fouling in forward osmosis membranes: The role of feed solution chemistry and membrane structural properties, Journal of Membrane Science, 460 (2014) 99-109.
[10] T.Y. Cath, A.E. Childress, M. Elimelech, Forward osmosis: Principles, applications, and recent developments, Journal of Membrane Science, 281 (2006) 70-87.
[11] N. Akther, A. Sodiq, A. Giwa, S. Daer, H.A. Arafat, S.W. Hasan, Recent advancements in forward osmosis desalination: A review, Chemical Engineering Journal, 281 (2015) 502-522.
[12] T.-S. Chung, S. Zhang, K.Y. Wang, J. Su, M.M. Ling, Forward osmosis processes: Yesterday, today and tomorrow, Desalination, 287 (2012) 78-81.
[13] S. Zhao, L. Zou, C.Y. Tang, D. Mulcahy, Recent developments in forward osmosis: Opportunities and challenges, Journal of Membrane Science, 396 (2012) 1-21.
[14] N. Akther, S. Daer, Q. Wei, I. Janajreh, S.W. Hasan, Synthesis of polybenzimidazole (PBI) forward osmosis (FO) membrane and computational fluid dynamics (CFD) modeling of concentration gradient across membrane surface, Desalination, 452 (2019) 17-28.
[15] R.K. McGovern, J.H. Lienhard V, On the potential of forward osmosis to energetically outperform reverse osmosis desalination, Journal of Membrane Science, 469 (2014) 245-250.
[16] D.L. Shaffer, J.R. Werber, H. Jaramillo, S. Lin, M. Elimelech, Forward osmosis: Where are we now?, Desalination, 356 (2015) 271-284.
[17] N. Akther, S. Daer, S.W. Hasan, Effect of flow rate, draw solution concentration and temperature on the performance of TFC FO membrane, and the potential use of RO reject brine as a draw solution in FO–RO hybrid systems, Desalination and Water Treatment, 136 (2018) 65-71.
[18] S. Zhang, K.Y. Wang, T.-S. Chung, H. Chen, Y.C. Jean, G. Amy, Well-constructed cellulose acetate membranes for forward osmosis: Minimized internal concentration polarization with an ultra-thin selective layer, Journal of Membrane Science, 360 (2010) 522-535.

[19] C.R. Martinetti, A.E. Childress, T.Y. Cath, High recovery of concentrated RO brines using forward osmosis and membrane distillation, Journal of Membrane Science, 331 (2009) 31-39.
[20] F.A. Siddiqui, Q. She, A.G. Fane, R.W. Field, Exploring the differences between forward osmosis and reverse osmosis fouling, Journal of Membrane Science, 565 (2018) 241-253.
[21] S.M. Ali, J.E. Kim, S. Phuntsho, A. Jang, J.Y. Choi, H.K. Shon, Forward osmosis system analysis for optimum design and operating conditions, Water Research, 145 (2018) 429-441.
[22] V.H. Tran, S. Lim, D.S. Han, N. Pathak, N. Akther, S. Phuntsho, H. Park, H.K. Shon, Efficient fouling control using outer-selective hollow fiber thin-film composite membranes for osmotic membrane bioreactor applications, Bioresource Technology, 282 (2019) 9-17.
[23] J.R. McCutcheon, R.L. McGinnis, M. Elimelech, A novel ammonia-carbon dioxide forward (direct) osmosis desalination process, Desalination, 174 (2005) 1-11.
[24] J.R. McCutcheon, M. Elimelech, Influence of concentrative and dilutive internal concentration polarization on flux behavior in forward osmosis, Journal of Membrane Science, 284 (2006) 237-247.
[25] J.R. Mccutcheon, M. Elimelech, Modeling water flux in forward osmosis: Implications for improved membrane design, AIChE Journal, 53 (2007) 1736-1744.
[26] J. Herron, Asymmetric forward osmosis membranes, in: H.T. Inc. (Ed.), Hydration Technologies Inc., USA, 2008.
[27] N.Y. Yip, A. Tiraferri, W.A. Phillip, J.D. Schiffman, M. Elimelech, High performance thin-film composite forward osmosis membrane, Environmental Science & Technology, 44 (2010) 3812–3818.
[28] J. Ren, J.R. McCutcheon, A new commercial thin film composite membrane for forward osmosis, Desalination, 343 (2014) 187-193.
[29] K.D. Vos, F.O. Burris, R.L. Riley, Kinetic study of the hydrolysis of cellulose acetate in the pH range of 2–10, Journal of Applied Polymer Science, 10 (1966) 825-832.
[30] W.J. Lau, S. Gray, T. Matsuura, D. Emadzadeh, J. Paul Chen, A.F. Ismail, A review on polyamide thin film nanocomposite (TFN) membranes: History, applications, challenges and approaches, Water Research, 80 (2015) 306-324.
[31] A.F. Ismail, M. Padaki, N. Hilal, T. Matsuura, W.J. Lau, Thin film composite membrane — Recent development and future potential, Desalination, 356 (2015) 140-148.
[32] J. Wei, C. Qiu, C.Y. Tang, R. Wang, A.G. Fane, Synthesis and characterization of flat-sheet thin film composite forward osmosis membranes, Journal of Membrane Science, 372 (2011) 292-302.
[33] N. Widjojo, T.-S. Chung, M. Weber, C. Maletzko, V. Warzelhan, The role of sulphonated polymer and macrovoid-free structure in the support layer for thin-film composite (TFC) forward osmosis (FO) membranes, Journal of Membrane Science, 383 (2011) 214-223.
[34] G. Han, T.-S. Chung, M. Toriida, S. Tamai, Thin-film composite forward osmosis membranes with novel hydrophilic supports for desalination, Journal of Membrane Science, 423–424 (2012) 543-555.
[35] Q. Liu, J. Li, Z. Zhou, J. Xie, J.Y. Lee, Hydrophilic mineral coating of membrane substrate for reducing internal concentration polarization (ICP) in forward osmosis, Scientific Reports, 6 (2016).
[36] C. Klaysom, S. Hermans, A. Gahlaut, S. Van Craenenbroeck, I.F.J. Vankelecom, Polyamide/Polyacrylonitrile (PA/PAN) thin film composite osmosis membranes: Film optimization, characterization and performance evaluation, Journal of Membrane Science, 445 (2013) 25-33.
[37] Z.-Y. Li, V. Yangali-Quintanilla, R. Valladares-Linares, Q. Li, T. Zhan, G. Amy, Flux patterns and membrane fouling propensity during desalination of seawater by forward osmosis, Water Research, 46 (2012) 195-204.

[38] E.A. Bell, T.E. Poynor, K.B. Newhart, J. Regnery, B.D. Coday, T.Y. Cath, Produced water treatment using forward osmosis membranes: Evaluation of extended-time performance and fouling, Journal of Membrane Science, 525 (2017) 77-88.
[39] Y. Chun, D. Mulcahy, L. Zou, I. Kim, A Short Review of Membrane Fouling in Forward Osmosis Processes, Membranes, 7 (2017) 30.
[40] X. Wang, Y. Zhao, B. Yuan, Z. Wang, X. Li, Y. Ren, Comparison of biofouling mechanisms between cellulose triacetate (CTA) and thin-film composite (TFC) polyamide forward osmosis membranes in osmotic membrane bioreactors, Bioresource Technology, 202 (2016) 50-58.
[41] L.M. Robeson, Correlation of separation factor versus permeability for polymeric membranes, Journal of Membrane Science, 62 (1991) 165-185.
[42] D. Li, Y. Yan, H. Wang, Recent advances in polymer and polymer composite membranes for reverse and forward osmosis processes, Progress in Polymer Science, 61 (2016) 104-155.
[43] J. Xiao, Y. Huang, C.W. Manke, Computational Design of Polymer Nanocomposite Coatings: A Multiscale Hierarchical Approach for Barrier Property Prediction, Industrial & Engineering Chemistry Research, 49 (2010) 7718-7727.
[44] A. Soroush, W. Ma, Y. Silvino, M.S. Rahaman, Surface modification of thin film composite forward osmosis membrane by silver-decorated graphene-oxide nanosheets, Environmental Science: Nano, 2 (2015) 395-405.
[45] N. Ma, J. Wei, R. Liao, C.Y. Tang, Zeolite-polyamide thin film nanocomposite membranes: Towards enhanced performance for forward osmosis, Journal of Membrane Science, 405 (2012) 149-157.
[46] B.-H. Jeong, E.M.V. Hoek, Y. Yan, A. Subramani, X. Huang, G. Hurwitz, A.K. Ghosh, A. Jawor, Interfacial polymerization of thin film nanocomposites: A new concept for reverse osmosis membranes, Journal of Membrane Science, 294 (2007) 1-7.
[47] A. Tiraferri, C.D. Vecitis, M. Elimelech, Covalent binding of single-walled carbon nanotubes to polyamide membranes for antimicrobial surface properties, ACS Applied Materials & Interfaces, 3 (2011) 2869-2877.
[48] H.M. Hegab, A. ElMekawy, T.G. Barclay, A. Michelmore, L. Zou, C.P. Saint, M. Ginic-Markovic, Effective in-situ chemical surface modification of forward osmosis membranes with polydopamine-induced graphene oxide for biofouling mitigation, Desalination, 385 (2016) 126-137.
[49] S. Karan, Z. Jiang, A.G. Livingston, Sub–10 nm polyamide nanofilms with ultrafast solvent transport for molecular separation, Science, 348 (2015) 1347-1351.
[50] G.-R. Xu, J.-M. Xu, H.-J. Feng, H.-L. Zhao, S.-B. Wu, Tailoring structures and performance of polyamide thin film composite (PA-TFC) desalination membranes via sublayers adjustment-a review, Desalination, 417 (2017) 19-35.
[51] N. Ma, J. Wei, S. Qi, Y. Zhao, Y. Gao, C.Y. Tang, Nanocomposite substrates for controlling internal concentration polarization in forward osmosis membranes, Journal of Membrane Science, 441 (2013) 54-62.
[52] M.J. Park, S. Phuntsho, T. He, G.M. Nisola, L.D. Tijing, X.-M. Li, G. Chen, W.-J. Chung, H.K. Shon, Graphene oxide incorporated polysulfone substrate for the fabrication of flat-sheet thin-film composite forward osmosis membranes, Journal of Membrane Science, 493 (2015) 496-507.
[53] H. Salehi, M. Rastgar, A. Shakeri, Anti-fouling and high water permeable forward osmosis membrane fabricated via layer by layer assembly of chitosan/graphene oxide, Applied Surface Science, 413 (2017) 99-108.
[54] L. Jin, Z. Wang, S. Zheng, B. Mi, Polyamide-crosslinked graphene oxide membrane for forward osmosis, Journal of Membrane Science, 545 (2018) 11-18.

[55] L. Dumée, J. Lee, K. Sears, B. Tardy, M. Duke, S. Gray, Fabrication of thin film composite poly(amide)-carbon-nanotube supported membranes for enhanced performance in osmotically driven desalination systems, Journal of Membrane Science, 427 (2013) 422-430.
[56] K. Goh, L. Setiawan, L. Wei, W. Jiang, R. Wang, Y. Chen, Fabrication of novel functionalized multi-walled carbon nanotube immobilized hollow fiber membranes for enhanced performance in forward osmosis process, Journal of Membrane Science, 446 (2013) 244-254.
[57] L. Wang, X. Song, T. Wang, S. Wang, Z. Wang, C. Gao, Fabrication and characterization of polyethersulfone/carbon nanotubes (PES/CNTs) based mixed matrix membranes (MMMs) for nanofiltration application, Applied Surface Science, 330 (2015) 118-125.
[58] X. Fan, Y. Liu, X. Quan, A novel reduced graphene oxide/carbon nanotube hollow fiber membrane with high forward osmosis performance, Desalination, (2018).
[59] J.-Y. Lee, S. Qi, X. Liu, Y. Li, F. Huo, C.Y. Tang, Synthesis and characterization of silica gel–polyacrylonitrile mixed matrix forward osmosis membranes based on layer-by-layer assembly, Separation and Purification Technology, 124 (2014) 207-216.
[60] J.-Y. Lee, Y. Wang, C.Y. Tang, F. Huo, Mesoporous silica gel–based mixed matrix membranes for improving mass transfer in forward osmosis: Effect of pore size of filler, Scientific reports, 5 (2015).
[61] M. Huang, Y. Chen, C.-H. Huang, P. Sun, J. Crittenden, Rejection and adsorption of trace pharmaceuticals by coating a forward osmosis membrane with TiO2, Chemical Engineering Journal, 279 (2015) 904-911.
[62] M. Amini, A. Rahimpour, M. Jahanshahi, Forward osmosis application of modified TiO2-polyamide thin film nanocomposite membranes, Desalination and Water Treatment, 57 (2016) 14013-14023.
[63] C. Zhang, M. Huang, L. Meng, B. Li, T. Cai, Electrospun polysulfone (PSf)/titanium dioxide (TiO2) nanocomposite fibers as substrates to prepare thin film forward osmosis membranes, Journal of Chemical Technology & Biotechnology, 92 (2017) 2090-2097.
[64] H. Luo, Q. Wang, T.C. Zhang, T. Tao, A. Zhou, L. Chen, X. Bie, A review on the recovery methods of draw solutes in forward osmosis, Journal of Water Process Engineering, 4 (2014) 212-223.
[65] D. Zhao, S. Chen, C.X. Guo, Q. Zhao, X. Lu, Multi-functional forward osmosis draw solutes for seawater desalination, Chinese Journal of Chemical Engineering, 24 (2016) 23-30.
[66] T. Alejo, M. Arruebo, V. Carcelen, V.M. Monsalvo, V. Sebastian, Advances in draw solutes for forward osmosis: Hybrid organic-inorganic nanoparticles and conventional solutes, Chemical Engineering Journal, 309 (2017) 738-752.
[67] Z. Xie, N. Nagaraja, L. Skillman, D. Li, G. Ho, Comparison of polysaccharide fouling in forward osmosis and reverse osmosis separations, Desalination, 402 (2017) 174-184.
[68] A. Bogler, S. Lin, E. Bar-Zeev, Biofouling of membrane distillation, forward osmosis and pressure retarded osmosis: Principles, impacts and future directions, Journal of Membrane Science, 542 (2017) 378-398.
[69] T.-S. Chung, X. Li, R.C. Ong, Q. Ge, H. Wang, G. Han, Emerging forward osmosis (FO) technologies and challenges ahead for clean water and clean energy applications, Current Opinion in Chemical Engineering, 1 (2012) 246-257.
[70] T.-S. Chung, L. Luo, C.F. Wan, Y. Cui, G. Amy, What is next for forward osmosis (FO) and pressure retarded osmosis (PRO), Separation and Purification Technology, 156 (2015) 856-860.
[71] L. Chekli, S. Phuntsho, J.E. Kim, J. Kim, J.Y. Choi, J.-S. Choi, S. Kim, J.H. Kim, S. Hong, J. Sohn, H.K. Shon, A comprehensive review of hybrid forward osmosis systems: Performance, applications and future prospects, Journal of Membrane Science, 497 (2016) 430-449.

[72] A.J. Ansari, F.I. Hai, W.E. Price, J.E. Drewes, L.D. Nghiem, Forward osmosis as a platform for resource recovery from municipal wastewater - A critical assessment of the literature, Journal of Membrane Science, 529 (2017) 195-206.
[73] I.L. Alsvik, M.-B. Hägg, Pressure retarded osmosis and forward osmosis membranes: Materials and methods, Polymers, 5 (2013) 303-327.
[74] P. Lu, Y. Gao, A. Umar, T. Zhou, J. Wang, Z. Zhang, L. Huang, Q. Wang, Recent advances in cellulose-based forward osmosis membrane, Science of Advanced Materials, 7 (2015) 2182-2192.
[75] W. Xu, Q. Chen, Q. Ge, Recent advances in forward osmosis (FO) membrane: Chemical modifications on membranes for FO processes, Desalination, 419 (2017) 101-116.
[76] J. Habel, M. Hansen, S. Kynde, N. Larsen, S.R. Midtgaard, G.V. Jensen, J. Bomholt, A. Ogbonna, K. Almdal, A. Schulz, C. Hélix-Nielsen, Aquaporin-Based Biomimetic Polymeric Membranes: Approaches and Challenges, Membranes, 5 (2015) 307-351.
[77] A. Giwa, N. Akther, V. Dufour, S.W. Hasan, A critical review on recent polymeric and nano-enhanced membranes for reverse osmosis, RSC Advances, 6 (2016) 8134-8163.
[78] M. Amini, M. Jahanshahi, A. Rahimpour, Synthesis of novel thin film nanocomposite (TFN) forward osmosis membranes using functionalized multi-walled carbon nanotubes, Journal of Membrane Science, 435 (2013) 233-241.
[79] X. Song, L. Wang, C.Y. Tang, Z. Wang, C. Gao, Fabrication of carbon nanotubes incorporated double-skinned thin film nanocomposite membranes for enhanced separation performance and antifouling capability in forward osmosis process, Desalination, 369 (2015) 1-9.
[80] D. Emadzadeh, W.J. Lau, M. Rahbari-Sisakht, H. Ilbeygi, D. Rana, T. Matsuura, A.F. Ismail, Synthesis, modification and optimization of titanate nanotubes-polyamide thin film nanocomposite (TFN) membrane for forward osmosis (FO) application, Chemical Engineering Journal, 281 (2015) 243-251.
[81] M. Ghanbari, D. Emadzadeh, W.J. Lau, S.O. Lai, T. Matsuura, A.F. Ismail, Synthesis and characterization of novel thin film nanocomposite (TFN) membranes embedded with halloysite nanotubes (HNTs) for water desalination, Desalination, 358 (2015) 33-41.
[82] M. Ghanbari, D. Emadzadeh, W.J. Lau, T. Matsuura, M. Davoody, A.F. Ismail, Super hydrophilic TiO2/HNT nanocomposites as a new approach for fabrication of high performance thin film nanocomposite membranes for FO application, Desalination, 371 (2015) 104-114.
[83] X. Song, L. Wang, L. Mao, Z. Wang, Nanocomposite membrane with different carbon nanotubes location for nanofiltration and forward osmosis applications, ACS Sustainable Chemistry & Engineering, 4 (2016) 2990-2997.
[84] W. Ding, Y. Li, M. Bao, J. Zhang, C. Zhang, J. Lu, Highly permeable and stable forward osmosis (FO) membrane based on the incorporation of Al2O3 nanoparticles into both substrate and polyamide active layer, RSC Advances, 7 (2017) 40311-40320.
[85] D. Ma, S.B. Peh, G. Han, S.B. Chen, Thin-film nanocomposite (TFN) membranes incorporated with super-hydrophilic metal–organic framework (MOF) UiO-66: Toward enhancement of water flux and salt rejection, ACS Applied Materials & Interfaces, 9 (2017) 7523-7534.
[86] A. Zirehpour, A. Rahimpour, M. Ulbricht, Nano-sized metal organic framework to improve the structural properties and desalination performance of thin film composite forward osmosis membrane, Journal of Membrane Science, 531 (2017) 59-67.
[87] Y.-H. Chiao, A. Sengupta, S.-T. Chen, S.-H. Huang, C.-C. Hu, W.-S. Hung, Y. Chang, X. Qian, S. Ranil Wickramasinghe, K.-R. Lee, J.-Y. Lai, Zwitterion augmented polyamide membrane for improved forward osmosis performance with significant antifouling characteristics, Separation and Purification Technology, (2018).

[88] N. Akther, S. Lim, V.H. Tran, S. Phuntsho, Y. Yang, T.-H. Bae, N. Ghaffour, H.K. Shon, The effect of Schiff base network on the separation performance of thin film nanocomposite forward osmosis membranes, Separation and Purification Technology, 217 (2019) 284-293.
[89] N. Niksefat, M. Jahanshahi, A. Rahimpour, The effect of SiO2 nanoparticles on morphology and performance of thin film composite membranes for forward osmosis application, Desalination, 343 (2014) 140-146.
[90] L. Shen, S. Xiong, Y. Wang, Graphene oxide incorporated thin-film composite membranes for forward osmosis applications, Chemical Engineering Science, 143 (2016) 194-205.
[91] D. Emadzadeh, M. Ghanbari, W.J. Lau, M. Rahbari-Sisakht, T. Matsuura, A.F. Ismail, B. Kruczek, Solvothermal synthesis of nanoporous TiO2: The impact on thin-film composite membranes for engineered osmosis application, Nanotechnology, 27 (2016) 345702.
[92] X. Wu, R.W. Field, J.J. Wu, K. Zhang, Polyvinylpyrrolidone modified graphene oxide as a modifier for thin film composite forward osmosis membranes, Journal of Membrane Science, 540 (2017) 251-260.
[93] A. Rahimpour, S.F. Seyedpour, S. Aghapour Aktij, M. Dadashi Firouzjaei, A. Zirehpour, A. Arabi Shamsabadi, S. Khoshhal Salestan, M. Jabbari, M. Soroush, Simultaneous improvement of antimicrobial, antifouling, and transport properties of forward osmosis membranes with immobilized highly-compatible polyrhodanine nanoparticles, Environmental Science & Technology, 52 (2018) 5246-5258.
[94] R. Ramezani Darabi, M. Jahanshahi, M. Peyravi, A support assisted by photocatalytic Fe3O4/ZnO nanocomposite for thin-film forward osmosis membrane, Chemical Engineering Research and Design, 133 (2018) 11-25.
[95] S.S. Eslah, S. Shokrollahzadeh, O.M. Jazani, A. Samimi, Forward osmosis water desalination: Fabrication of graphene oxide-polyamide/polysulfone thin-film nanocomposite membrane with high water flux and low reverse salt diffusion, Separation Science and Technology, 53 (2018) 573-583.
[96] M. Rastgar, A. Shakeri, A. Bozorg, H. Salehi, V. Saadattalab, Highly-efficient forward osmosis membrane tailored by magnetically responsive graphene oxide/Fe3O4 nanohybrid, Applied Surface Science, 441 (2018) 923-935.
[97] M.G.N. Perera, Y.R. Galagedara, Y. Ren, M. Jayaweera, Y. Zhao, R. Weerasooriya, Fabrication of fullerenol-incorporated thin-film nanocomposite forward osmosis membranes for improved desalination performances, Journal of Polymer Research, 25 (2018) 199.
[98] M. Rezaei-DashtArzhandi, M.H. Sarrafzadeh, P.S. Goh, a. L{Rezaei-DashtArzhandi, W. J., A.F. Ismail, M.A. Mohamed, Development of novel thin film nanocomposite forward osmosis membranes containing halloysite/graphitic carbon nitride nanoparticles towards enhanced desalination performance, Desalination, 447 (2018) 18-28.
[99] S.F. Seyedpour, A. Rahimpour, A.A. Shamsabadi, M. Soroush, Improved performance and antifouling properties of thin-film composite polyamide membranes modified with nano-sized bactericidal graphene quantum dots for forward osmosis, Chemical Engineering Research and Design, 139 (2018) 321-334.
[100] X. Wu, M. Shaibani, S.J.D. Smith, K. Konstas, M.R. Hill, H. Wang, K. Zhang, Z. Xie, Microporous carbon from fullerene impregnated porous aromatic frameworks for improving the desalination performance of thin film composite forward osmosis membranes, Journal of Materials Chemistry A, 6 (2018) 11327-11336.
[101] E.E. McLeary, J.C. Jansen, F. Kapteijn, Zeolite based films, membranes and membrane reactors: Progress and prospects, Microporous and Mesoporous Materials, 90 (2006) 198-220.
[102] C.T. Kresge, M.E. Leonowicz, W.J. Roth, J.C. Vartuli, J.S. Beck, Ordered mesoporous molecular sieves synthesized by a liquid-crystal template mechanism, Nature, 359 (1992) 710.

[103] P.S. Goh, A.F. Ismail, B.C. Ng, Carbon nanotubes for desalination: Performance evaluation and current hurdles, Desalination, 308 (2013) 2-14.
[104] K. Goh, H.E. Karahan, L. Wei, T.-H. Bae, A.G. Fane, R. Wang, Y. Chen, Carbon nanomaterials for advancing separation membranes: A strategic perspective, Carbon, 109 (2016) 694-710.
[105] D. Mattia, K.P. Lee, F. Calabrò, Water permeation in carbon nanotube membranes, Current Opinion in Chemical Engineering, 4 (2014) 32-37.
[106] R. Das, S.B. Abd Hamid, M.E. Ali, A.F. Ismail, M.S.M. Annuar, S. Ramakrishna, Multifunctional carbon nanotubes in water treatment: The present, past and future, Desalination, 354 (2014) 160-179.
[107] R. Das, M.E. Ali, S.B.A. Hamid, S. Ramakrishna, Z.Z. Chowdhury, Carbon nanotube membranes for water purification: A bright future in water desalination, Desalination, 336 (2014) 97-109.
[108] B. Corry, Designing carbon nanotube membranes for efficient water desalination, The Journal of Physical Chemistry B, 112 (2008) 1427-1434.
[109] H.J. Kim, K. Choi, Y. Baek, D.-G. Kim, J. Shim, J. Yoon, J.-C. Lee, High-performance reverse osmosis CNT/polyamide nanocomposite membrane by controlled interfacial interactions, ACS Applied Materials & Interfaces, 6 (2014) 2819-2829.
[110] A. Rahimpour, M. Jahanshahi, S. Khalili, A. Mollahosseini, A. Zirepour, B. Rajaeian, Novel functionalized carbon nanotubes for improving the surface properties and performance of polyethersulfone (PES) membrane, Desalination, 286 (2012) 99-107.
[111] C. Chen, Q.H. Yang, Y. Yang, W. Lv, Y. Wen, P.X. Hou, M. Wang, H.M. Cheng, Self-assembled free-standing graphite oxide membrane, Advanced Materials, 21 (2009) 3007-3011.
[112] W.S. Hung, Q.F. An, M. De Guzman, H.Y. Lin, S.H. Huang, W.R. Liu, C.C. Hu, K.R. Lee, J.Y. Lai, Pressure-assisted self-assembly technique for fabricating composite membranes consisting of highly ordered selective laminate layers of amphiphilic graphene oxide, Carbon, 68 (2014) 670-677.
[113] H.M. Hegab, L. Zou, Graphene oxide-assisted membranes: Fabrication and potential applications in desalination and water purification, Journal of Membrane Science, 484 (2015) 95-106.
[114] M. Hu, B. Mi, Layer-by-layer assembly of graphene oxide membranes via electrostatic interaction, Journal of Membrane Science, 469 (2014) 80-87.
[115] H.M. Hegab, L. Zou, Graphene oxide-assisted membranes: Fabrication and potential applications in desalination and water purification, Journal of Membrane Science, 484 (2015) 95-106.
[116] K.A. Mahmoud, B. Mansoor, A. Mansour, M. Khraisheh, Functional graphene nanosheets: The next generation membranes for water desalination, Desalination, 356 (2015) 208-225.
[117] J.Y. Chong, B. Wang, K. Li, Graphene oxide membranes in fluid separations, Current Opinion in Chemical Engineering, 12 (2016) 98-105.
[118] S.G. Kim, D.H. Hyeon, J.H. Chun, B.-H. Chun, S.H. Kim, Novel thin nanocomposite RO membranes for chlorine resistance, Desalination and Water Treatment, 51 (2013) 6338-6345.
[119] B.M. Ganesh, A.M. Isloor, A.F. Ismail, Enhanced hydrophilicity and salt rejection study of graphene oxide-polysulfone mixed matrix membrane, Desalination, 313 (2013) 199-207.
[120] J. Zhang, Z. Xu, W. Mai, C. Min, B. Zhou, M. Shan, Y. Li, C. Yang, Z. Wang, X. Qian, Improved hydrophilicity, permeability, antifouling and mechanical performance of PVDF composite ultrafiltration membranes tailored by oxidized low-dimensional carbon nanomaterials, Journal of Materials Chemistry A, 1 (2013) 3101-3111.

[121] H. Zhao, L. Wu, Z. Zhou, L. Zhang, H. Chen, Improving the antifouling property of polysulfone ultrafiltration membrane by incorporation of isocyanate-treated graphene oxide, Physical Chemistry Chemical Physics, 15 (2013) 9084-9092.
[122] L. Yu, Y. Zhang, B. Zhang, J. Liu, H. Zhang, C. Song, Preparation and characterization of HPEI-GO/PES ultrafiltration membrane with antifouling and antibacterial properties, Journal of Membrane Science, 447 (2013) 452-462.
[123] P. Salehian, T.-S. Chung, Thermally treated ammonia functionalized graphene oxide/polyimide membranes for pervaporation dehydration of isopropanol, Journal of Membrane Science, 528 (2017) 231-242.
[124] N. Wang, S. Ji, J. Li, R. Zhang, G. Zhang, Poly(vinyl alcohol)–graphene oxide nanohybrid "pore-filling" membrane for pervaporation of toluene/n-heptane mixtures, Journal of Membrane Science, 455 (2014) 113-120.
[125] N. Wang, S. Ji, G. Zhang, J. Li, L. Wang, Self-assembly of graphene oxide and polyelectrolyte complex nanohybrid membranes for nanofiltration and pervaporation, Chemical Engineering Journal, 213 (2012) 318-329.
[126] Y. Yuan, X. Gao, Y. Wei, X. Wang, J. Wang, Y. Zhang, C. Gao, Enhanced desalination performance of carboxyl functionalized graphene oxide nanofiltration membranes, Desalination, 405 (2017) 29-39.
[127] H. Huang, Y. Ying, X. Peng, Graphene oxide nanosheet: An emerging star material for novel separation membranes, Journal of Materials Chemistry A, 2 (2014) 13772-13782.
[128] G. Liu, W. Jin, N. Xu, Graphene-based membranes, Chemical Society Reviews, 44 (2015) 5016-5030.
[129] A.F. Faria, C. Liu, M. Xie, F. Perreault, L.D. Nghiem, J. Ma, M. Elimelech, Thin-film composite forward osmosis membranes functionalized with graphene oxide–silver nanocomposites for biofouling control, Journal of Membrane Science, 525 (2017) 146-156.
[130] A. Inurria, P. Cay-Durgun, D. Rice, H. Zhang, D.-K. Seo, M.L. Lind, F. Perreault, Polyamide thin-film nanocomposite membranes with graphene oxide nanosheets: Balancing membrane performance and fouling propensity, Desalination, 451 (2018) 139-147.
[131] F. Perreault, H. Jaramillo, M. Xie, M. Ude, L.D. Nghiem, M. Elimelech, Biofouling mitigation in forward osmosis using graphene oxide functionalized thin-film composite membranes, Environmental Science & Technology, 50 (2016) 5840-5848.
[132] Q. Chen, L.M. Peng, Structure and applications of titanate and related nanostructures, International Journal of Nanotechnology, 4 (2007) 44-65.
[133] R. Wang, G. Jiang, Y. Ding, Y. Wang, X. Sun, X. Wang, W. Chen, Photocatalytic activity of heterostructures based on TiO2 and halloysite nanotubes, ACS Applied Materials & Interfaces, 3 (2011) 4154-4158.
[134] J. Zhang, Y. Zhang, Y. Chen, L. Du, B. Zhang, H. Zhang, J. Liu, K. Wang, Preparation and characterization of novel polyethersulfone hybrid ultrafiltration membranes bending with modified halloysite nanotubes loaded with silver nanoparticles, Industrial & Engineering Chemistry Research, 51 (2012) 3081-3090.
[135] M. Ghanbari, D. Emadzadeh, W.J. Lau, T. Matsuura, A.F. Ismail, Synthesis and characterization of novel thin film nanocomposite reverse osmosis membranes with improved organic fouling properties for water desalination, RSC Advances, 5 (2015) 21268-21276.
[136] M. Ghanbari, D. Emadzadeh, W.J. Lau, H. Riazi, D. Almasi, A.F. Ismail, Minimizing structural parameter of thin film composite forward osmosis membranes using polysulfone/halloysite nanotubes as membrane substrates, Desalination, 377 (2016) 152-162.
[137] R. Kumar, H. Al-Jabli, S. Al-Haddad, M. Al-Rughaib, J. Samuel, Modified titanate nanotubes incorporated polyamide layer for the fabrication of fouling control thin-film nanocomposite forward osmosis membranes, Desalination and Water Treatment, 69 (2017) 56-64.

[138] S.-Y. Ding, J. Gao, Q. Wang, Y. Zhang, W.-G. Song, C.-Y. Su, W. Wang, Construction of covalent organic framework for catalysis: Pd/COF-LZU1 in Suzuki–Miyaura coupling reaction, Journal of the American Chemical Society, 133 (2011) 19816-19822.
[139] I. Tiscornia, I. Kumakiri, R. Bredesen, C. Téllez, J. Coronas, Microporous titanosilicate ETS-10 membrane for high pressure CO2 separation, Separation and Purification Technology, 73 (2010) 8-12.
[140] C. Li, S. Li, L. Tian, J. Zhang, B. Su, M.Z. Hu, Covalent organic frameworks (COFs)-incorporated thin film nanocomposite (TFN) membranes for high-flux organic solvent nanofiltration (OSN), Journal of Membrane Science, 572 (2019) 520-531.
[141] S. Sorribas, P. Gorgojo, C. Téllez, J. Coronas, A.G. Livingston, High Flux Thin Film Nanocomposite Membranes Based on Metal–Organic Frameworks for Organic Solvent Nanofiltration, Journal of the American Chemical Society, 135 (2013) 15201-15208.
[142] X.-L. Liu, Y.-S. Li, G.-Q. Zhu, Y.-J. Ban, L.-Y. Xu, W.-S. Yang, An organophilic pervaporation membrane derived from metal–organic framework nanoparticles for efficient recovery of bio-alcohols, Angewandte Chemie International Edition, 50 (2011) 10636-10639.
[143] A. Kasik, Y.S. Lin, Organic solvent pervaporation properties of MOF-5 membranes, Separation and Purification Technology, 121 (2014) 38-45.
[144] A. Car, C. Stropnik, K.-V. Peinemann, Hybrid membrane materials with different metal–organic frameworks (MOFs) for gas separation, Desalination, 200 (2006) 424-426.
[145] J.-Y. Lee, Q. She, F. Huo, C.Y. Tang, Metal–organic framework-based porous matrix membranes for improving mass transfer in forward osmosis membranes, Journal of Membrane Science, 492 (2015) 392-399.
[146] A. Zirehpour, A. Rahimpour, S. Khoshhal, M.D. Firouzjaei, A.A. Ghoreyshi, The impact of MOF feasibility to improve the desalination performance and antifouling properties of FO membranes, RSC Advances, 6 (2016) 70174-70185.
[147] Y. Cui, Y. Yue, G. Qian, B. Chen, Luminescent functional metal–organic frameworks, Chemical Reviews, 112 (2012) 1126-1162.
[148] H. Furukawa, K.E. Cordova, M. O'Keeffe, O.M. Yaghi, The chemistry and applications of metal-organic frameworks, Science, 341 (2013).
[149] X. Feng, X. Ding, D. Jiang, Covalent organic frameworks, Chemical Society Reviews, 41 (2012) 6010-6022.
[150] J.-R. Li, J. Sculley, H.-C. Zhou, Metal–organic frameworks for separations, Chemical Reviews, 112 (2012) 869-932.
[151] S.-P. Sun, T.-S. Chung, Outer-Selective Pressure-Retarded Osmosis Hollow Fiber Membranes from Vacuum-Assisted Interfacial Polymerization for Osmotic Power Generation, Environmental Science & Technology, 47 (2013) 13167-13174.
[152] G.S. Lai, W.J. Lau, P.S. Goh, Y.H. Tan, B.C. Ng, A.F. Ismail, A novel interfacial polymerization approach towards synthesis of graphene oxide-incorporated thin film nanocomposite membrane with improved surface properties, Arabian Journal of Chemistry, 12 (2019) 75-87.
[153] E. Yang, A.B. Alayande, C.-M. Kim, J.-h. Song, I.S. Kim, Laminar reduced graphene oxide membrane modified with silver nanoparticle-polydopamine for water/ion separation and biofouling resistance enhancement, Desalination, 426 (2018) 21-31.
[154] E. Yang, M.-H. Ham, H.B. Park, C.-M. Kim, J.-h. Song, I.S. Kim, Tunable semi-permeability of graphene-based membranes by adjusting reduction degree of laminar graphene oxide layer, Journal of Membrane Science, 547 (2018) 73-79.
[155] A. Tiraferri, Y. Kang, E.P. Giannelis, M. Elimelech, Highly hydrophilic thin-film composite forward osmosis membranes functionalized with surface-tailored nanoparticles, ACS Applied Materials & Interfaces, 4 (2012) 5044-5053.

[156] A. Tiraferri, Y. Kang, E.P. Giannelis, M. Elimelech, Superhydrophilic thin-film composite forward osmosis membranes for organic fouling control: Fouling behavior and antifouling mechanisms, Environmental Science & Technology, 46 (2012) 11135-11144.
[157] S. Zhang, G. Qiu, Y.P. Ting, T.-S. Chung, Silver–PEGylated dendrimer nanocomposite coating for anti-fouling thin film composite membranes for water treatment, Colloids and Surfaces A: Physicochemical and Engineering Aspects, 436 (2013) 207-214.
[158] H.M. Hegab, A. ElMekawy, T.G. Barclay, A. Michelmore, L. Zou, C.P. Saint, M. Ginic-Markovic, Fine-tuning the surface of forward osmosis membranes via grafting graphene oxide: Performance patterns and biofouling propensity, ACS Applied Materials & Interfaces, 7 (2015) 18004-18016.
[159] H. Jin, Y. Huang, H. Li, P. Yu, Y. Luo, Fabrication of BaSO4-based mineralized thin-film composite polysulfone/polyamide membranes for enhanced performance in a forward osmosis process, RSC Advances, 5 (2015) 79774-79782.
[160] F. Perreault, M.E. Tousley, M. Elimelech, Thin-film composite polyamide membranes functionalized with biocidal graphene oxide nanosheets, Environmental Science & Technology Letters, 1 (2014) 71-76.
[161] A. Soroush, W. Ma, M. Cyr, M.S. Rahaman, B. Asadishad, N. Tufenkji, In situ silver decoration on graphene oxide-treated thin film composite forward osmosis membranes: Biocidal properties and regeneration potential, Environmental Science & Technology Letters, 3 (2016) 13-18.
[162] H. Jin, F. Rivers, H. Yin, T. Lai, P. Cay-Durgun, A. Khosravi, M.L. Lind, P. Yu, Synthesis of AgCl mineralized thin film composite polyamide membranes to enhance performance and antifouling properties in forward osmosis, Industrial & Engineering Chemistry Research, 56 (2017) 1064-1073.
[163] Y. Huang, P. Cay-Durgun, T. Lai, P. Yu, M.L. Lind, Phenol removal from water by polyamide and AgCl mineralized thin-film composite forward osmosis membranes, Industrial & Engineering Chemistry Research, 57 (2018) 7021-7029.
[164] L. Qi, Y. Hu, Z. Liu, X. An, E. Bar-Zeev, Improved anti-biofouling performance of thin -film composite forward-osmosis membranes containing passive and active moieties, Environmental Science & Technology, 52 (2018) 9684-9693.
[165] M. Qiu, C. He, Novel zwitterion-silver nanocomposite modified thin-film composite forward osmosis membrane with simultaneous improved water flux and biofouling resistance property, Applied Surface Science, 455 (2018) 492-501.
[166] M. Huang, Y. Chen, C.-H. Huang, P. Sun, J. Crittenden, Rejection and adsorption of trace pharmaceuticals by coating a forward osmosis membrane with TiO2, Chemical Engineering Journal, 279 (2015) 904-911.
[167] D. Qin, Z. Liu, D. Delai Sun, X. Song, H. Bai, A new nanocomposite forward osmosis membrane custom-designed for treating shale gas wastewater, Scientific Reports, 5 (2015) 14530.
[168] P. Lu, S. Liang, T. Zhou, T. Xue, X. Mei, Q. Wang, Layered double hydroxide nanoparticle modified forward osmosis membranes via polydopamine immobilization with significantly enhanced chlorine and fouling resistance, Desalination, (2017).
[169] S.J. Zaidi, K.A. Mauritz, M.K. Hassan, Membrane Surface Modification and Functionalization, in: M.A. Jafar Mazumder, H. Sheardown, A. Al-Ahmed (Eds.) Functional Polymers, Springer International Publishing, Cham, 2018, pp. 1-26.
[170] Y. Wang, R. Ou, Q. Ge, H. Wang, T. Xu, Preparation of polyethersulfone/carbon nanotube substrate for high-performance forward osmosis membrane, Desalination, 330 (2013) 70-78.

[171] M. Tian, Y.-N. Wang, R. Wang, Synthesis and characterization of novel high-performance thin film nanocomposite (TFN) FO membranes with nanofibrous substrate reinforced by functionalized carbon nanotubes, Desalination, 370 (2015) 79-86.
[172] S. Morales-Torres, C.M.P. Esteves, J.L. Figueiredo, A.M.T. Silva, Thin-film composite forward osmosis membranes based on polysulfone supports blended with nanostructured carbon materials, Journal of Membrane Science, 520 (2016) 326-336.
[173] H.-g. Choi, M. Son, H. Choi, Integrating seawater desalination and wastewater reclamation forward osmosis process using thin-film composite mixed matrix membrane with functionalized carbon nanotube blended polyethersulfone support layer, Chemosphere, 185 (2017) 1181-1188.
[174] Y.-H. Pan, Q.-Y. Zhao, L. Gu, Q.-Y. Wu, Thin film nanocomposite membranes based on imologite nanotubes blended substrates for forward osmosis desalination, Desalination, 421 (2017) 160-168.
[175] D. Ma, G. Han, S.B. Peh, S.B. Chen, Water-Stable Metal–Organic Framework UiO-66 for Performance Enhancement of Forward Osmosis Membranes, Industrial & Engineering Chemistry Research, 56 (2017) 12773-12782.
[176] X. Zhang, L. Shen, C.-Y. Guan, C.-X. Liu, W.-Z. Lang, Y. Wang, Construction of SiO2@MWNTs incorporated PVDF substrate for reducing internal concentration polarization in forward osmosis, Journal of Membrane Science, 564 (2018) 328-341.
[177] W.J. Lee, P.S. Goh, W.J. Lau, C.S. Ong, A.F. Ismail, Antifouling zwitterion embedded forward osmosis thin film composite membrane for highly concentrated oily wastewater treatment, Separation and Purification Technology, (2018).
[178] D. Emadzadeh, W. Lau, A. Ismail, Synthesis of thin film nanocomposite forward osmosis membrane with enhancement in water flux without sacrificing salt rejection, Desalination, 330 (2013) 90-99.
[179] D. Emadzadeh, W.J. Lau, T. Matsuura, N. Hilal, A.F. Ismail, The potential of thin film nanocomposite membrane in reducing organic fouling in forward osmosis process, Desalination, 348 (2014) 82-88.
[180] D. Emadzadeh, W. Lau, T. Matsuura, A. Ismail, M. Rahbari-Sisakht, Synthesis and characterization of thin film nanocomposite forward osmosis membrane with hydrophilic nanocomposite support to reduce internal concentration polarization, Journal of Membrane Science, 449 (2014) 74-85.
[181] X. Liu, H.Y. Ng, Fabrication of layered silica–polysulfone mixed matrix substrate membrane for enhancing performance of thin-film composite forward osmosis membrane, Journal of Membrane Science, 481 (2015) 148-163.
[182] Y. Wang, R. Ou, H. Wang, T. Xu, Graphene oxide modified graphitic carbon nitride as a modifier for thin film composite forward osmosis membrane, Journal of Membrane Science, 475 (2015) 281-289.
[183] Z.X. Low, Q. Liu, E. Shamsaei, X. Zhang, H. Wang, Preparation and characterization of thin-film composite membrane with nanowire-modified support for forward osmosis process, Membranes, 5 (2015) 136.
[184] P. Lu, S. Liang, T. Zhou, X. Mei, Y. Zhang, C. Zhang, A. Umar, Q. Wang, Layered double hydroxide/graphene oxide hybrid incorporated polysulfone substrate for thin-film nanocomposite forward osmosis membranes, RSC Advances, 6 (2016) 56599-56609.
[185] N.-N. Bui, J.R. McCutcheon, Nanoparticle-embedded nanofibers in highly permselective thin-film nanocomposite membranes for forward osmosis, Journal of Membrane Science, 518 (2016) 338-346.
[186] M. Obaid, Z.K. Ghouri, O.A. Fadali, K.A. Khalil, A.A. Almajid, N.A.M. Barakat, Amorphous SiO2 NP-incorporated poly(vinylidene fluoride) electrospun nanofiber membrane

for high flux forward osmosis desalination, ACS Applied Materials & Interfaces, 8 (2016) 4561-4574.
[187] P. Lu, S. Liang, L. Qiu, Y. Gao, Q. Wang, Thin film nanocomposite forward osmosis membranes based on layered double hydroxide nanoparticles blended substrates, Journal of Membrane Science, 504 (2016) 196-205.
[188] W. Kuang, Z. Liu, H. Yu, G. Kang, X. Jie, Y. Jin, Y. Cao, Investigation of internal concentration polarization reduction in forward osmosis membrane using nano-CaCO3 particles as sacrificial component, Journal of Membrane Science, 497 (2016) 485-493.
[189] S. Lim, M.J. Park, S. Phuntsho, L.D. Tijing, G.M. Nisola, W.-G. Shim, W.-J. Chung, H.K. Shon, Dual-layered nanocomposite substrate membrane based on polysulfone/graphene oxide for mitigating internal concentration polarization in forward osmosis, Polymer, 110 (2017) 36-48.
[190] T. Sirinupong, W. Youravong, D. Tirawat, W.J. Lau, G.S. Lai, A.F. Ismail, Synthesis and characterization of thin film composite membranes made of PSF-TiO2/GO nanocomposite substrate for forward osmosis applications, Arabian Journal of Chemistry, (2017).
[191] R.R. Darabi, M. Peyravi, M. Jahanshahi, A.A. Qhoreyshi Amiri, Decreasing ICP of forward osmosis (TFN-FO) membrane through modifying PES-Fe3O4 nanocomposite substrate, Korean Journal of Chemical Engineering, 34 (2017) 2311-2324.
[192] M. Rastgar, A. Shakeri, A. Bozorg, H. Salehi, V. Saadattalab, Impact of nanoparticles surface characteristics on pore structure and performance of forward osmosis membranes, Desalination, 421 (2017) 179-189.
[193] M. Tian, Y.-N. Wang, R. Wang, A.G. Fane, Synthesis and characterization of thin film nanocomposite forward osmosis membranes supported by silica nanoparticle incorporated nanofibrous substrate, Desalination, 401 (2017) 142-150.
[194] M.L. Lind, A.K. Ghosh, A. Jawor, X. Huang, W. Hou, Y. Yang, E.M.V. Hoek, Influence of zeolite crystal size on zeolite-polyamide thin film nanocomposite membranes, Langmuir, 25 (2009) 10139-10145.
[195] M. Fathizadeh, A. Aroujalian, A. Raisi, Effect of added NaX nano-zeolite into polyamide as a top thin layer of membrane on water flux and salt rejection in a reverse osmosis process, Journal of Membrane Science, 375 (2011) 88-95.
[196] H. Huang, X. Qu, H. Dong, L. Zhang, H. Chen, Role of NaA zeolites in the interfacial polymerization process towards a polyamide nanocomposite reverse osmosis membrane, RSC Advances, 3 (2013) 8203-8207.
[197] M.M. Pendergast, A.K. Ghosh, E.M.V. Hoek, Separation performance and interfacial properties of nanocomposite reverse osmosis membranes, Desalination, 308 (2013) 180-185.
[198] Y. Huang, H. Jin, P. Yu, Y. Luo, Polyamide thin-film composite membrane based on nano-silica modified polysulfone microporous support layer for forward osmosis, Desalination and Water Treatment, 57 (2016) 20177-20187.
[199] X. Li, K.Y. Wang, B. Helmer, T.-S. Chung, Thin-film composite membranes and formation mechanism of thin-film layers on hydrophilic cellulose acetate propionate substrates for forward osmosis processes, Industrial & Engineering Chemistry Research, 51 (2012) 10039-10050.
[200] Y. Wang, R. Ou, Q. Ge, H. Wang, T. Xu, Preparation of polyethersulfone/carbon nanotube substrate for high-performance forward osmosis membrane, Desalination, 330 (2013) 70-78.
[201] M. Hu, B. Mi, Enabling graphene oxide nanosheets as water separation membranes, Environmental Science & Technology, 47 (2013) 3715-3723.
[202] G.S. Lai, W.J. Lau, S.R. Gray, T. Matsuura, R.J. Gohari, M.N. Subramanian, S.O. Lai, C.S. Ong, A.F. Ismail, D. Emazadah, M. Ghanbari, A practical approach to synthesize

1888 polyamide thin film nanocomposite (TFN) membranes with improved separation properties for
1889 water/wastewater treatment, Journal of Materials Chemistry A, 4 (2016) 4134-4144.
1890 [203] S. Stankovich, D.A. Dikin, G.H.B. Dommett, K.M. Kohlhaas, E.J. Zimney, E.A. Stach,
1891 R.D. Piner, S.T. Nguyen, R.S. Ruoff, Graphene-based composite materials, Nature, 442 (2006)
1892 282.
1893 [204] G.S. Lai, W.J. Lau, P.S. Goh, A.F. Ismail, N. Yusof, Y.H. Tan, Graphene oxide
1894 incorporated thin film nanocomposite nanofiltration membrane for enhanced salt removal
1895 performance, Desalination, 387 (2016) 14-24.
1896 [205] S. Zinadini, A.A. Zinatizadeh, M. Rahimi, V. Vatanpour, H. Zangeneh, Preparation of a
1897 novel antifouling mixed matrix PES membrane by embedding graphene oxide nanoplates,
1898 Journal of Membrane Science, 453 (2014) 292-301.
1899 [206] D. Yang, J. Li, Z. Jiang, L. Lu, X. Chen, Chitosan/TiO2 nanocomposite pervaporation
1900 membranes for ethanol dehydration, Chemical Engineering Science, 64 (2009) 3130-3137.
1901 [207] S. Yang, J.-S. Gu, H.-Y. Yu, J. Zhou, S.-F. Li, X.-M. Wu, L. Wang, Polypropylene
1902 membrane surface modification by RAFT grafting polymerization and TiO2 photocatalysts
1903 immobilization for phenol decomposition in a photocatalytic membrane reactor, Separation
1904 and Purification Technology, 83 (2011) 157-165.
1905 [208] A. Razmjou, E. Arifin, G. Dong, J. Mansouri, V. Chen, Superhydrophobic modification
1906 of TiO2 nanocomposite PVDF membranes for applications in membrane distillation, Journal
1907 of Membrane Science, 415-416 (2012) 850-863.
1908 [209] M. Safarpour, A. Khataee, V. Vatanpour, Thin film nanocomposite reverse osmosis
1909 membrane modified by reduced graphene oxide/TiO2 with improved desalination
1910 performance, Journal of Membrane Science, 489 (2015) 43-54.
1911 [210] E.-J. Lee, A.K. An, T. He, Y.C. Woo, H.K. Shon, Electrospun nanofiber membranes
1912 incorporating fluorosilane-coated TiO2 nanocomposite for direct contact membrane
1913 distillation, Journal of Membrane Science, 520 (2016) 145-154.
1914 [211] D. Emadzadeh, W.J. Lau, T. Matsuura, M. Rahbari-Sisakht, A.F. Ismail, A novel thin
1915 film composite forward osmosis membrane prepared from PSf–TiO2 nanocomposite substrate
1916 for water desalination, Chemical Engineering Journal, 237 (2014) 70-80.
1917 [212] V.C. Farmer, A.R. Fraser, J.M. Tait, Synthesis of imogolite: A tubular aluminium silicate
1918 polymer, Journal of the Chemical Society, Chemical Communications, (1977) 462-463.
1919 [213] G.N.B. Baroña, M. Choi, B. Jung, High permeate flux of PVA/PSf thin film composite
1920 nanofiltration membrane with aluminosilicate single-walled nanotubes, Journal of Colloid and
1921 Interface Science, 386 (2012) 189-197.
1922 [214] G.N.B. Baroña, J. Lim, M. Choi, B. Jung, Interfacial polymerization of polyamide-
1923 aluminosilicate SWNT nanocomposite membranes for reverse osmosis, Desalination, 325
1924 (2013) 138-147.
1925 [215] C. Deng, Q.G. Zhang, G.L. Han, Y. Gong, A.M. Zhu, Q.L. Liu, Ultrathin self-assembled
1926 anionic polymer membranes for superfast size-selective separation, Nanoscale, 5 (2013)
1927 11028-11034.
1928 [216] R.C. Ong, T.-S. Chung, J.S. de Wit, B.J. Helmer, Novel cellulose ester substrates for
1929 high performance flat-sheet thin-film composite (TFC) forward osmosis (FO) membranes,
1930 Journal of Membrane Science, 473 (2015) 63-71.
1931 [217] P. Sukitpaneenit, T.-S. Chung, High Performance Thin-Film Composite Forward
1932 Osmosis Hollow Fiber Membranes with Macrovoid-Free and Highly Porous Structure for
1933 Sustainable Water Production, Environmental Science & Technology, 46 (2012) 7358-7365.
1934 [218] B. Khorshidi, T. Thundat, B.A. Fleck, M. Sadrzadeh, Thin film composite polyamide
1935 membranes: parametric study on the influence of synthesis conditions, RSC Advances, 5
1936 (2015) 54985-54997.

[219] P. Gorgojo, S. Karan, H.C. Wong, M.F. Jimenez-Solomon, J.T. Cabral, A.G. Livingston, Ultrathin Polymer Films with Intrinsic Microporosity: Anomalous Solvent Permeation and High Flux Membranes, Advanced Functional Materials, 24 (2014) 4729-4737.
[220] X. Zhao, J. Li, C. Liu, A novel TFC-type FO membrane with inserted sublayer of carbon nanotube networks exhibiting the improved separation performance, Desalination, 413 (2017) 176-183.
[221] W. Zhao, H. Liu, Y. Liu, M. Jian, L. Gao, H. Wang, X. Zhang, Thin-Film Nanocomposite Forward-Osmosis Membranes on Hydrophilic Microfiltration Support with an Intermediate Layer of Graphene Oxide and Multiwall Carbon Nanotube, ACS Applied Materials & Interfaces, 10 (2018) 34464-34474.
[222] Z. Zhou, Y. Hu, C. Boo, Z. Liu, J. Li, L. Deng, X. An, High-Performance Thin-Film Composite Membrane with an Ultrathin Spray-Coated Carbon Nanotube Interlayer, Environmental Science & Technology Letters, 5 (2018) 243-248.
[223] H.-g. Choi, A.A. Shah, S.-E. Nam, Y.-I. Park, H. Park, Thin-film composite membranes comprising ultrathin hydrophilic polydopamine interlayer with graphene oxide for forward osmosis, Desalination, 449 (2019) 41-49.
[224] Y. Wang, X. Li, S. Zhao, Z. Fang, D. Ng, C. Xie, H. Wang, Z. Xie, Thin-Film Composite Membrane with Interlayer Decorated Metal–Organic Framework UiO-66 toward Enhanced Forward Osmosis Performance, Industrial & Engineering Chemistry Research, 58 (2019) 195-206.
[225] Y.H. Cho, J. Han, S. Han, M.D. Guiver, H.B. Park, Polyamide thin-film composite membranes based on carboxylated polysulfone microporous support membranes for forward osmosis, Journal of Membrane Science, 445 (2013) 220-227.
[226] C. Kong, A. koushima, T. Kamada, T. Shintani, M. Kanezashi, T. Yoshioka, T. Tsuru, Enhanced performance of inorganic-polyamide nanocomposite membranes prepared by metal-alkoxide-assisted interfacial polymerization, Journal of Membrane Science, 366 (2011) 382-388.
[227] Y.-x. Jia, H.-l. Li, M. Wang, L.-y. Wu, Y.-d. Hu, Carbon nanotube: Possible candidate for forward osmosis, Separation and Purification Technology, 75 (2010) 55-60.
[228] A. Sharma, S. Kumar, B. Tripathi, M. Singh, Y.K. Vijay, Aligned CNT/Polymer nanocomposite membranes for hydrogen separation, International Journal of Hydrogen Energy, 34 (2009) 3977-3982.
[229] X. Li, A. Sotto, J. Li, B. Van der Bruggen, Progress and perspectives for synthesis of sustainable antifouling composite membranes containing in situ generated nanoparticles, Journal of Membrane Science, 524 (2017) 502-528.
[230] B. Kim, G. Gwak, S. Hong, Review on methodology for determining forward osmosis (FO) membrane characteristics: Water permeability (A), solute permeability (B), and structural parameter (S), Desalination, 422 (2017) 5-16.
[231] T.Y. Cath, M. Elimelech, J.R. McCutcheon, R.L. McGinnis, A. Achilli, D. Anastasio, A.R. Brady, A.E. Childress, I.V. Farr, N.T. Hancock, J. Lampi, L.D. Nghiem, M. Xie, N.Y. Yip, Standard Methodology for Evaluating Membrane Performance in Osmotically Driven Membrane Processes, Desalination, 312 (2013) 31-38.
[232] A. Tiraferri, N.Y. Yip, A.P. Straub, S. Romero-Vargas Castrillon, M. Elimelech, A method for the simultaneous determination of transport and structural parameters of forward osmosis membranes, Journal of Membrane Science, 444 (2013) 523-538.